R&D for Future 100 kton Scale Liquid Argon Detectors

A. Marchionni
ETH Zurich, 101 Raemistrasse, CH-8092 Zurich, Switzerland

Abstract
Large liquid argon (LAr) detectors, up to 100 kton scale, are presently being considered for proton decay searches and neutrino astrophysics as well as far detectors for the next generation of long baseline neutrino oscillation experiments, aiming at neutrino mass hierarchy determination and CP violation searches in the leptonic sector. These detectors rely on the possibility of maintaining large LAr masses stably at cryogenic conditions with low thermal losses and of achieving long drifts of the ionization charge, so to minimize the number of readout channels per unit volume. Many R&D initiatives are being undertaken throughout the world, following somewhat different concepts for the final detector design, but with many common basic R&D issues.

1 Introduction

A high granularity detector of large size, with a fine sampling down to a few percent of a radiation length, and with tracking and calorimetric capabilities, would be ideal to perform next generation neutrino physics, providing a clean identification of ν_e induced charged current interactions. Bubble chambers have clearly shown their potentiality as neutrino detectors, though limited in size, while larger size calorimetric detectors have been suffering from coarse granularity and limitations in the identification of the electromagnetic component in neutrino interactions. A clean measurement of electrons is becoming crucial in long baseline neutrino oscillation experiments driven by ∼MW proton beams for the determination of the θ_{13} mixing angle, the neutrino mass hierarchy and ultimately in the search for CP violation in the leptonic sector. Large liquid argon time projection chambers (LAr TPC), up to ∼100 kton size, have been proposed as far dectors in these experiments (Refs. [1]– [6]). LAr TPCs, when compared to water Cerenkov detectors, allow lower momentum thresholds for the identification of heavier particles, notably protons, and are predicted to have higher electron identification efficiency with better rejection of the π^0 background.

A LAr detector of 100 kton size, if installed underground even at moderate depth, would extend the search for proton decay via modes favored by supersymmetric grand unified models (e.g. $p \longrightarrow K^+\bar{\nu}$) up to $\sim 10^{35}$ years, having from 5 to 10 times the efficiency of water Cerenkov detectors for such decays [7]. The synergy between precise detectors for long neutrino baseline experiments, proton decay and astrophysical neutrinos (see Refs. [8, 9]) is essential for a realistic proposal of a 100 kton scale LAr detector.

The LAr TPC technique, first proposed by C. Rubbia in 1977 [10], has been developed in the last 20 years by the ICARUS collaboration (see Fig. 1), culminating with a 300 ton detector (T300) successfully operated on surface [11] and a 600 ton detector (T600) installed undeground in LNGS along the CNGS neutrino beam, now almost ready to be commissioned.

The use of LAr TPCs as neutrino detectors was pioneered already ten years ago by the ICARUS collaboration with the exposure of a 50 liters LAr TPC [12] on the WANF neutrino beam (see Fig. 2). Given the revived interest for the LAr technique, nowadays several groups have already placed [13] or are planning to expose [14] somewhat bigger LAr detectors on neutrino beams, of 170 and 130 liters active volumes, respectively. About 20k neutrino interactions are expected by spring 2010 in the ArgoNeut detector installed on the NuMI neutrino beam at FNAL in front of the MINOS Near Detector (see Fig. 3).

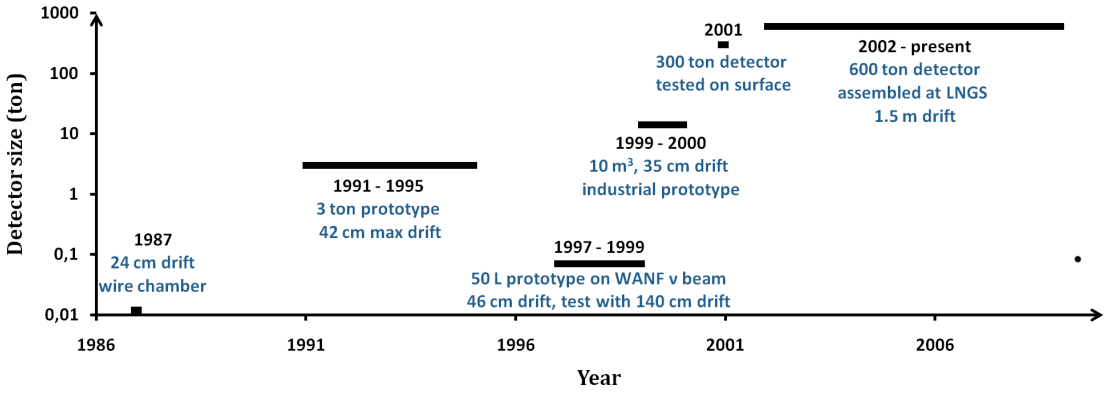

Fig. 1: The ICARUS R&D steps towards kton size LAr detectors

Recently proposed LAr detectors require a step in size of about a factor 100 with respect to the ICARUS detector. Though challenging, this is not unrealistic over a period of ∼10 years and a well thought R&D path. In Section 2 we will present the main technical issues in scaling from an ICARUS-like detector to a ∼100 times larger device and in Section 3 we will describe in some detail the ongoing R&D work. Different design concepts have been proposed by different groups for 100 kton scale LAr TPCs. These are summarized in Section 4, together with the proposed R&D paths to get to the final detectors.

2 Technical issues for large LAr TPCs

Fundamental physics questions would be answered by operating a 50–100 kton active volume LAr TPC detector. Extrapolation to ∼100 times larger size than the ICARUS T600 detector requires:

1. longer drift path for the collection of the ionization charge, in order to reduce the number of readout channels per unit volume and the dead spaces introduced by the readout electrodes and cathode structures. As discussed in Section 4, drift lengths ranging from a few to about 10 times the 1.5 m ICARUS T600 drift length have been proposed. Longer drift lengths can only be achieved if the ionization charge from minimum ionizing particles at the maximum drift distance is still detectable and suitable high voltage systems, that could produce the required drift field (0.5–1 kV/cm), are available.
2. larger cryogenic vessels, suitable for undeground construction and operation, with low enough thermal losses to afford the costs of a long term cryogenic operation and of sufficient tightness to keep electronegative impurities within a few tens of parts per trillion (ppt). Recirculation and purification systems in liquid and gas phases will be necessary to achieve and maintain the required

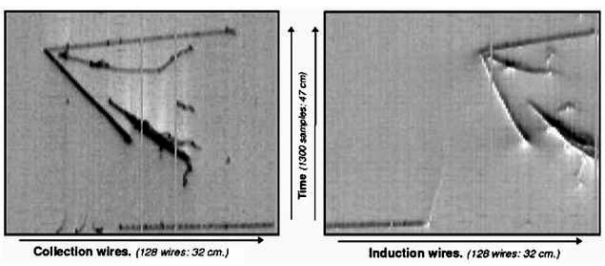

Fig. 2: An event recorded in the ICARUS 50 L chamber [12]

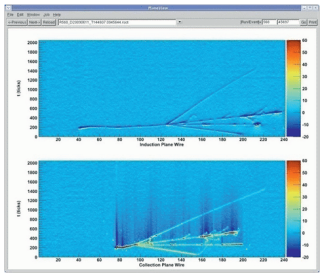

Fig. 3: An event in the ArgoNeut chamber on the NuMI beam at FNAL [13]

LAr purity. Even in a modular approach, where the ∼100 kton LAr mass is achieved by multiple smaller detectors, LAr vessels of more than ten times the ICARUS size are required. If on one hand this represents a challenge for the engineering design of the vessel, on the other hand a larger volume/surface ratio is an advantage for maintaining the detector in cryogenic conditions and for the purity of the LAr itself.

The main technical issues are summarized in Fig. 4. An active R&D program pursued by several groups in different regions of the world is already addressing these issues, as described in detail in the following Section.

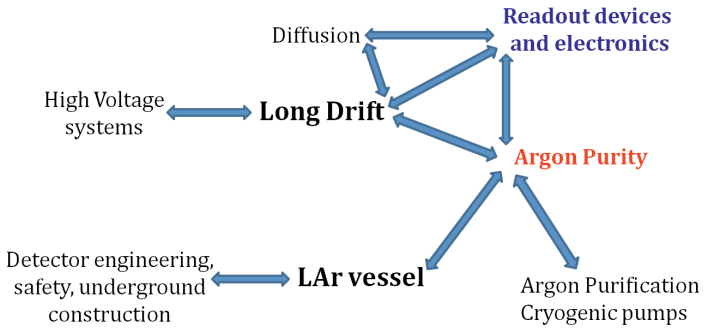

Fig. 4: Technical issues for large LAr TPCs

3 R&D items

3.1 Readout devices and electronics

The choice of readout methods of the ionization charge released in LAr and the corresponding electronics plays an essential role in the design of a long drift LAr detector. For a given LAr purity, longer drifts are affordable only if the signal of a minimum ionizing particle, collected from the maximum drift distance, is sufficiently larger than the electronic noise (typically a signal/noise ratio of at least 10 is necessary), posing stringent requirements on the electronics and somehow favoring the use of readout devices where the released ionization charge is amplified.

The standard method for reading out the ionization charge in LAr, decribed in Refs. [10, 15], and pioneered by the ICARUS collaboration, makes use of three parallel wire planes, with wires at different angles. The first two wire planes are fully transparent to the drifting electrons and detect a signal induced by the moving electrons, while the third plane acts as a collecting electrode. By digitizing the signal as a function of the drift time, each wire plane provides a two dimensional view of the event, with one coordinate given by the wire number and the other by the drift time. Extrapolation of this technique to ∼100 kton LAr vessels is not straightforward. It would require very long wires if a single LAr vessel is considered, resulting, in addition to mechanical issues with long wires, in larger capacitances and increased noise, or, in order to limit the length of the wires, it would demand a modularized approach with several smaller independent vessels or a segmentation of the LAr volume with several independent readout wire planes. The increased capacitance for long wires has to be compensated by widening the wire pitch, as in [16], in order to regain a good signal/noise ratio.

The operation of a LAr TPC in double phase (liquid-vapor), as suggested in [1], opens the possibility of amplification of the ionization charge in the pure argon vapor phase. A very active and promising R&D program is being conducted by several groups on thick GEMs (THGEM, macroscopic hole multipliers manufactured with standard PCB techniques) as charge amplifying devices (see Ref. [17] for a recent review). They have been successfully operated in noble gases [18], without any added quenching gas, and in double-phase argon detectors [19, 20]. THGEMs represent a robust and economic way to realize large area detectors, suitable for cryogenic operation.

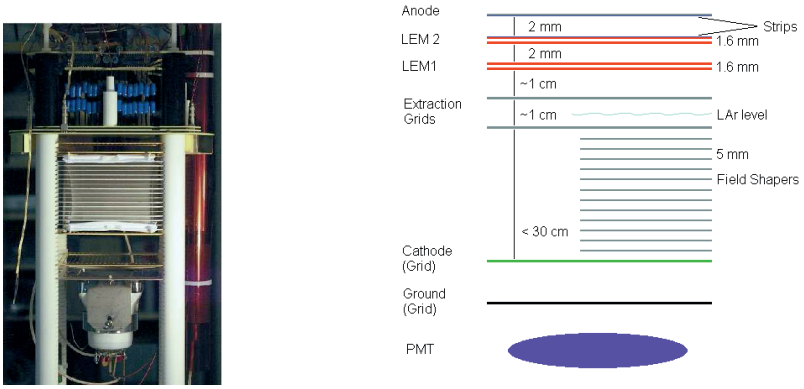

Fig. 5: Thick GEM LAr TPC: (left) photo of the test setup at CERN; (right) schematic of the chamber

A 3 liters prototype double-phase argon TPC has been successfully operated with single and double stage THGEMs, for the first time with imaging capability, as described in Refs. [22, 23]. Figure 5 shows the test setup with a double stage THGEM (otherwise called LEM, Large Electron Multiplier) of 10×10 cm^2. The amplified electron signal is readout via two orthogonal coordinates, the segmented upper electrode of the THGEM itself followed by a segmented anode, both with 6 mm wide strips. Half of the charge is usually collected on the THGEM electrode, while the remaining half reaches the anode. This novel device, which will be referred to as LAr THGEM-TPC, has been proposed in Ref. [1] for large size LAr detectors. Examples of cosmic muons are shown in Fig. 6a for a single stage 1 mm thick THGEM. A very good signal/noise ratio of ~ 60 is apparent from the digitized signals recorded by the THGEM and anode 6 mm wide strips. This configuration provides, for a potential difference of 3.6 kV across the THGEM, an effective charge gain of $\sim$2-3 for each of the two readout electrodes. The distribution of released charge per unit length from reconstructed cosmic muons using the anode signals is shown in Fig. 6b with a superimposed fitted Landau distribution. Larger charge gains of about 10 have been achieved with a double stage THGEM of 1.6 mm thickness [23]. Installation of a $\sim$0.5 m^2 THGEM in the ArDM experiment [24] is foreseen in the next few months. The process of industrialization for the production of many squared meters of THGEMs detectors, necessary in large size LAr THGEM-TPCs as well as other applications, is being pursued by the RD51 Collaboration at CERN [21].

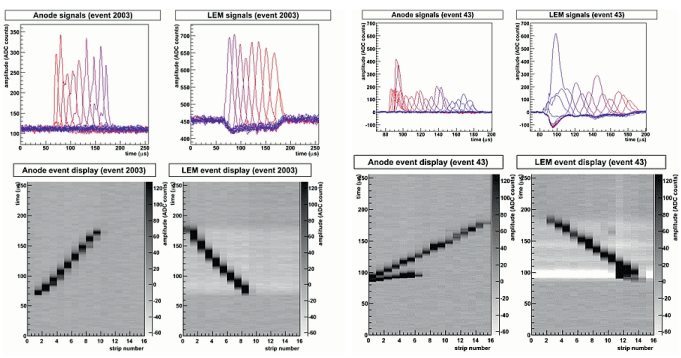

(a) Crossing muon events: (top) electronic signals; (bottom) displays of drift time vs position

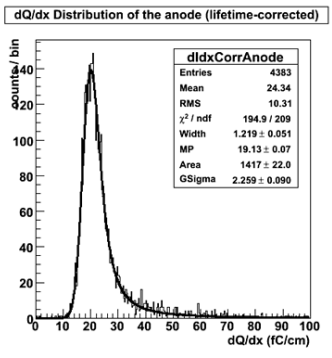

(b) Landau distribution from crossing muons

Fig. 6: Performance of 1 mm thick single stage thick GEM operating at 3.6 kV

The basic design of preamplifiers with multiple low noise JFETs at the input stage, connected in parallel to match a high detector capacitance, has been first employed by the ICARUS collaboration for the charge readout of a LAr TPC [25] and successfully adopted by other groups. The measurements

shown in Fig. 6 make use of a custom hybrid preamplifier [22] with a signal to noise ratio of 10 for 1 fC input charge and 200 pF input capacitance. While this performance is the state of the art for this technology, such a design is not directly transferable to an ASIC design, with a consequent cost reduction, because of the use of discrete JFET components. Attempts to reach similar noise performances by making use of ASIC preamplifiers based on CMOS technology, operated at cryogenic temperatures inside the detector vessel, are currently underway (see Refs. [13, 26]. This solution also allows to minimize the length, and consequently the capacitance, of the cables between the readout electrodes and the preamplifiers. This is particularly important in some of the designs of large size LAr TPCs, because it provides freedom in the location of the readout electrodes. Low power digitizers and multiplexers inside the cryogenic vessel have been proposed in [13] as a way to largely reduce the number of feedthroughs.

Since argon is a very good scintillator, recently attempts have been made to detect the released ionization charge in LAr by a radioactive source through the secondary scintillation light produced when ionization electrons are driven into the holes of a THGEM, where a high electric field is present [27]. Signals from an Fe^{55} source have been observed with good resolution in a double-phase argon setup: the scintillation light produced by the electrons extracted from the liquid phase and drifted into the holes of 1.5 mm thick THGEM, operating between 2.1 kV and 3.4 kV, has been detected by a single 1 mm^2 silicon photomultiplier, coated with a wavelength shifter (tetraphenyl butadiene). Extrapolation of this technique to large size LAr TPCs with tracking resolutions of a few mm would require an array of photosensors mounted behind the THGEM plane, calling for substantial R&D on low cost photosensors. A first attempt to produce secondary scintillation light in the holes of the THGEM directly immersed in liquid argon requires more work to fully comprehend the preliminary observations. Signals from the Fe^{55} source have been observed, but for a very narrow range of the applied high voltage across the THGEM ($\sim$10 kV) and with considerable worsening in resolution.

3.2 LAr vessels

Traditionally high purity LAr vessels have been built as stainless steel vacuum insulated dewars, where the inner vessel is also evacuable. Such devices are not scalable to the required dimensions of the envisioned LAr detectors (> 10000 m^3), if built with standard techniques. A design trying to maintain the features of vacuum insulation and evacuable vessels for very large containers, with regularly spaced mechanical reinforcements, is described in Section 4.

The ICARUS T600 vessel, which was designed with the main criteria to be transportable on the Italian highways, utilizes an aluminum LAr vessel with evacuated, honeycomb-structured insulation panels.

Very large cryogenic vessels, with a more favorable volume/surface ratio, can make use of passive insulation. Industrial tanks for the containment of liquefied natural gas (LNG, > 95% CH_4), up to volumes of 200000 m^3, are built as non-evacuable nickel steel tanks, making use of perlite or foam glass as thermal insulation. Several groups have proposed to use similar vessels for the containment of LAr (see Refs. [28], [29], [1], [2]) based on the following facts: the boiling points of LAr and CH_4 are quite close, 87.3 and 111.6 K respectively; the latent heat of vaporization per unit volume is the same for both liquids within 5%; with a LAr density 3.3 times higher than liquefied CH_4, the tank needs to withstand 3.3 times higher hydrostatic pressure, which is achievable with thicker steel; thermal losses of $\sim$5 W/m^2 are achievable with passive insulation methods ($\sim$ 1.5 m thick perlite insulation), resulting in a boil-off of only 0.04%/day for a 100 kton LAr vessel.

A corrugated stainless steel/Invar membrane tank, as recently built for an underground pilot plant for containment of LN_2 [30], is also being considered [13].

In such designs the LAr vessel is non-evacuable and it requires purification from air before proceeding with the LAr filling. Preliminary tests on small tanks have already been conducted at FNAL [31] and at KEK [14] with gas argon purging, reaching O_2 contaminations less than 50 ppm within a

few hours of purging. Large scale tests are foreseen at CERN by the ETH Zurich group with a 6 m^3 device, and at FNAL with a 20 ton LAr tank (LAPD project). The purification procedure starting from air will also provide a check of the tightness of the non-evacuable vessels through the measurement of the residual O_2 and N_2 contaminations in the argon gas.

3.3 High voltage systems

A drift field of 0.5 kV/cm, the nominal value in the ICARUS T300 detector over a drift distance of 1.5 m, corresponds to a drift velocity of the ionization electrons of 1.6 mm/μs. In such a range the drift velocity is already not linear with the electric field, still drift velocities of 2 mm/μs could be achieved with drift fields of 1 kV/cm, allowing to collect a higher percentage of ionization charge for a given electron lifetime.

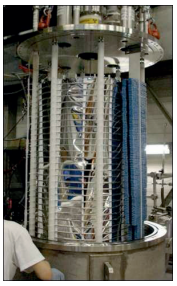

Fig. 7: Voltage multiplier in the ArDM experiment

Fig. 8: Material test stand at FNAL

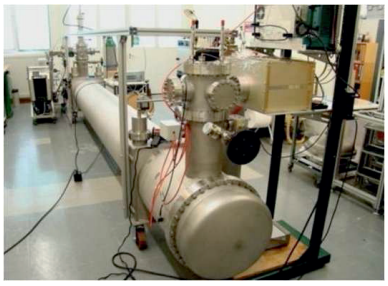

Fig. 9: Horizontal 5 m drift test stup at CERN

The need for longer drift paths and relatively high drift velocities drives towards higher high voltage values. At least few 100 kV are envisioned for large LAr detectors. The ICARUS HV feedthrough [11] has been tested up to 150 kV, and the design could in principle be extrapolated to larger values. A different approach has been followed in the ArDM experiment [24, 32], where a 210 stage Cockroft-Walton voltage multiplier, directly immersed in LAr, with a maximum voltage of $\sim$2 kV/stage and providing a drift field of $\sim$4 kV/cm, has been built as shown in Fig. 7, and will be tested in the next few months. Smaller prototypes have already reached voltages of $\sim$120 kV during short term tests in LAr. This technique could be used to generate higher voltages (MV like), in a range where commercial HV power supplies are not available, to produce drift fields of 1 kV/cm over a $\sim$10 m distance, posing less stringent requirements than in the ArDM case on the voltage multiplier.

3.4 Argon purity

The relatively low drift velocity in LAr, combined with drift paths of at least a few meters, implies drift times $\geq$ few ms. During such long drifts it is essential to ensure the collection of a high percentage of the ionization charge, the electron lifetime τ being directly related to the O_2-equivalent impurity concentration ρ by $\tau(\mu s) = 300/\rho[ppb]$. The concentration of electronegative impurities must be kept at the level of a few tens of ppt to reach electron lifetimes of the order of 10 ms. Since the fundamental achievements of the ICARUS collaboration, argon purity remains an important R&D subject, mainly focusing on LAr purification techniques, qualification of materials and monitors of argon purity.

The LAr recirculation system of a $\sim$100 kton scale LAr detector will need many cryogenic pumps working in parallel, with small thermal losses and without compromising the purity of the argon. Every small LAr setup offers the opportunity to test new schemes and new devices for LAr recirculation systems and cryogenic pumps, as for example in the ArDM experiment. Custom made purification cartridges have been developed for ArDM, based on CuO powder, and at FNAL, using copper-coated alumina granules [33]. Such cartridges are easily regenerable at about 250°C in a stream of Ar/H_2 gas. At FNAL electron

lifetimes of $\sim$10 ms, at the upper limit of the instrument range, have been routinely obtained with such cartridges.

In a 120 liters LAr TPC test facility at the INFN-LNL laboratory [34], making use of a commercial Oxysorb/Hydrosorb filter as in the ICARUS T300 detector, an eletron lifetime of $(21.4^{+7.3}_{-4.3})$ ms has been achieved for several weeks. Both [23] and [34] stress the importance of purifying or removing the argon gas during the initial phase of the detector cooling, because it is possibly contaminated by outgassing.

At FNAL a material test facility has been developed to test a number of materials commonly used in detector construction [35] (see Fig. 8). No effect on the electron lifetime was measured when the materials were immersed in LAr, but, when positioned in the warmer region of the vapor phase (at $\sim$ 200 K), a strong decrease of the electron lifetime was observed, correlated with an increase of water concentration in the vapor phase. It is inferred that water is responsible for the decrease of the lifetime and that water concentrations in the liquid phase at the level of 10 ppt affect the electron lifetime.

A novel monitoring and calibration system, exploiting UV laser ionization in LAr, has been developed by the University of Bern [36]. A pulsed ultraviolet Nd-YAG laser, working on the 4th harmonic with a wavelength of 266 nm corresponding to 4.66 eV photons, produces tracks in LAr with a signal-to-noise ratio of 80 for 20 mJ laser beam energy. This device could be used for electron lifetime determination, but also for calibration and monitoring of large LAr masses. Straight tracks, laser generated, would provide a measurement of the uniformity of the drift field and the drift velocity.

3.5 Long drifts

Electron drifts of at least a few meters are necessary for the realization of a realistic 100 kton scale LAr detector, even if built in a modular way. Full scale measurements of long drifts are necessary to assess the effects of signal attenuation and charge diffusion, and at the same time they represent a test of the high voltage systems and of the capability to achieve and maintain the necessary LAr purity.

An horizontal drift setup of 5 m has been fully assembled at CERN (see Fig. 9 [37]), where it is being commissioned, while a vertical drift setup, again of 5 m, is under construction at the University of Bern. A more ambitious 10 m long vertical drift test is presently being contemplated at KEK, in a $\sim$30 m^3 vessel.

3.6 Large magnetized LAr volumes

Traditionally, bubble chambers and calorimetric neutrino detectors have been magnetized, in order to get a measurement of at least the muon momentum. These detectors also allow, by measuring the muon charge, the determination of the minority antineutrino (neutrino) component in wide band neutrino (antineutrino) beams, and the identification of charmed particles through their semileptonic decays. The presence of a magnetic field is essential in case of a neutrino beam from a neutrino factory for the identification of the so-called right and wrong sign leptons. Water Cerenkov detectors are not compatible with being operated in a magnetic field, making impossible, for example, the separate measurement of neutrino and antineutrino components of atmospheric neutrinos in such detectors.

The excellent tracking and calorimetric capabilities of a LAr TPC allow the measurement of particle energies for contained events. Even in case of through-going particles, their momenta can de determined up to a few GeV by means of multiple scattering. The possibility to magnetize large LAr TPCs has been discussed in Refs. [38, 39] mainly motivated by the measurement of the sign of the leptons. While relatively low fields (B$\gtrsim$0.1 T) are sufficient to determine the charge of muon tracks at least a few meters long, higher fields (B$\gtrsim$1 T) are necessary for the determination of the charge of electrons of a few GeV, since they start showering quite early in LAr (14 cm radiation length) [38]. A first proposal in Ref. [39] considered a huge vertical warm solenoid enclosing the LAr volume, surrounded by an iron iron yoke for the flux return. The warm coil would dissipate 17 MW for a field B=0.2 T, raising questions for the thermal insulation of the LAr vessel. To avoid this problem Ref. [40] proposes to immerse

a superconducting solenoid directly into the LAr vessel, possibly built out of High T_c superconductor cable, which could be operated at a temperature substantially larger than 4 K and possibly at the LAr temperature. Since HTS cables find many technological applications, e.g. Superconducting Magnetic Energy Storage, this is a rapidly developing market which needs to be carefully monitored.

A parameter directly connected with the complexity of a magnet is its total stored energy. A 100 kton LAr detector, magnetized at the maximum contemplated field of B=1 T, would have a stored magnetic energy of 30 GJ, about a factor ten higher than the energy stored in the solenoid of the CMS experiment at LHC. This is an extrapolation that might not be unrealistic, but that certainly requires dedicated engineering studies.

4 Summary of the main design concepts

Motivated by the necessity of large detectors for neutrino physics, proton decay and the observation of astrophysical neutrinos, several designs of large LAr detectors, up to ∼100 kton scale, have appeared in the last several years (see Refs. [1, 41], [2], [39, 42], [5, 16], [13]).

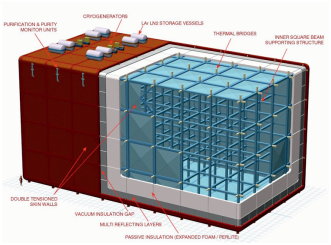

Fig. 10: Evacuable cryostat concept

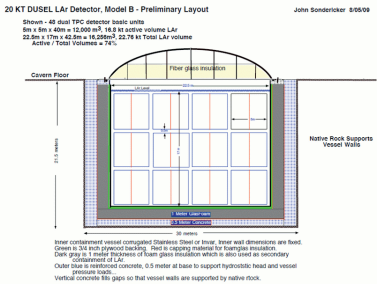

Fig. 11: LBNE cryostat concept

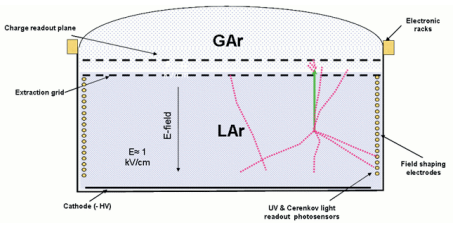

Fig. 12: GLACIER design concept

Reference [42] proposes scalable LAr TPC detectors based on an array of 3-dimensional cube frames immersed in a common LAr volume (see Fig. 10). This mechanical structure, if on one side complicates the construction of the readout devices, has been designed to allow evacuation of the inner vessel and consequently to preventively check its tightness. The design assumes a double wall cryostat, with vacuum insulation around the cold vessel.

Within the LBNE project in the US, it is being developed a conceptual design for an initial LAr module of 20 kton, to be installed in the DUSEL laboratory [13]. A total active mass of 50 to 100 kton would be achieved by the construction of multiple 20 kton modules. Figure 11 shows one design concept, with large rectangular TPC modules stacked inside a corrugated stainless steel/Invar membrane tank, using the cavern walls as support.

The MicroBooNE experiment at FNAL [43], with 100 ton LAr active volume, is considered an important step in the development of LAr TPCs in the US. In particular MicroBooNE will test the achievable purity when filling the vessel with LAr without evacuation, by initially purging with gaseous argon. The MicroBoone collaboration will implement hybrid JFET preampliers working in cold argon gas, investigating at the same time the development of cold CMOS electronics in LAr.

A single LAr module of 100 kton, denominated GLACIER, has been proposed in Ref. [1, 41] (see Fig. 12), with an almost total active LAr mass. The vessel is a cylindrical cyrogenic tank based on industrial LNG technology, providing an excellent volume/surface ratio, thus minimizing thermal losses and the effect of outgassing from the container walls. In order to reach 100 kton LAr mass, a single cylinder of 70 m diameter and 20 m height is being considered, with a single long vertical drift at high drift field (∼1 kV/cm), provided by an immersed Cockroft-Walton voltage multiplier. With a corresponding electron drift velocity of 2 mm/μs, this would allow better than 30% charge collection over

20 m drift for an electron lifetime of 10 ms. The charge loss during such long drifts can be compensated by operating the device in double-phase argon and by using charge amplification in pure argon gas by THGEMs, as described in Section 3.1.

As part of the R&D path to successfully design and propose a GLACIER-like detector, in addition to the R&D projects already described, it is proposed to expose a LAr TPC detector of about 6 m^3, operated in double-phase, to test beams in CERN SPS North Area [44] and to construct an engineering prototype of 1 kton [41], that could provide important physics outputs. A 1 kton detector, realized as a cylinder of 12 m diameter and 10 m height, is the largest possible detector that minimizes construction timescale and costs, as well as the extrapolation to 100 kton. All tank and LAr purification issues would be addressed by such a device and only a factor two extrapolation in drift length would be required for the final 100 kton tank. Underground construction and operation of a GLACIER-like tank, including all safety issues, is being studied as part of the LAGUNA design study [45] for specific european sites.

5 Conclusions

A 100 kton scale LAr detector aims at physics with discovery potential: the mass ordering of neutrinos, CP violation in the leptonic sector, proton decay, and more generally addressing fundamental physics at the Grand Unified scale. Such a detector, if built in Europe, would clearly benefit from a neutrino beam from CERN. A large choice of underground facilities at different baselines is being studied in the LAGUNA project.

Several proposals for large LAr TPCs have been put forward in different regions of the world, following somewhat different design concepts, but with many basic R&D issues in common. R&D for LAr, first pioneered by the ICARUS collaboration at CERN, is now being actively pursued in Europe, US and Japan. The ICARUS T600 detector, representing the first large scale LAr underground installation, is about to be commissioned and the ArgoNeut chamber on the NuMI neutrino beam at FNAL is recording neutrino interactions.

Some noteworthy R&D results for large scale detectors have been achieved in these last years: a 3 liters LAr THGEM-TPC prototype operated in double-phase has been shown to be able to achieve a better signal/noise ratio, new methods and technologies to purify LAr have resulted in lifetimes in excess of 10 ms, novel devices to monitor argon purity and drift velocities over large LAr masses have been developed. R&D on cold electronics, with far reaching consequences, is just started.

While engineering studies on the assembly and operation of 100 kton scale LAr vessels in underground locations are proceeding, several smaller scale setups will start operation in the next few years, for tests of novel high voltage systems, large scale operation of double-phase argon TPCs, full scale measurements of long drifts in LAr, large scale test of argon purification in non-evacuable vessels. The results from these setups will be essential to proceed with a reliable proposal and a sound cost estimate for a 100 kton scale LAr detector. Such a detector will probably require the construction of a full engineering prototype of 1 kton scale, which by itself would provide interesting physics output if located on a short-baseline neutrino beam.

Acknowledgements

I warmly acknowledge useful discussions with B. Baller, A. Rubbia and F. Sergiampietri and the many interactions with my colleagues from ETH Zurich and the LAr KEK group.

References

[1] A. Rubbia, *Experiments for CP-violation: A giant liquid argon scintillation, Cerenkov and charge imaging experiment?*, arXiv:hep-ph/0402110.

[2] L. Bartoszek *et al.*, *FLARE: Fermilab liquid argon experiments*, arXiv:hep-ex/0408121.

[3] A. Meregaglia and A. Rubbia, *Neutrino oscillation physics at an upgraded CNGS with large next generation liquid argon TPC detectors*, JHEP **0611** (2006) 032 [arXiv:hep-ph/0609106].

[4] V. Barger *et al.*, *Report of the US long baseline neutrino experiment study*, arXiv:0705.4396 [hep-ph].

[5] B. Baibussinov *et al.*, *A new, very massive modular Liquid Argon Imaging Chamber to detect low energy off-axis neutrinos from the CNGS beam. (Project MODULAr)*, Astropart. Phys. **29** (2008) 174 [arXiv:0704.1422 [hep-ph]].

[6] A. Badertscher *et al.*, *A Possible Future Long Baseline Neutrino and Nucleon Decay Experiment with a 100 kton Liquid Argon TPC at Okinoshima using the J-PARC Neutrino Facility*, arXiv:0804.2111 [hep-ph].

[7] A. Bueno *et al.*, *Nucleon decay searches with large liquid argon TPC detectors at shallow depths: Atmospheric neutrinos and cosmogenic backgrounds*, JHEP **0704** (2007) 041 [arXiv:hep-ph/0701101].

[8] I. Gil Botella and A. Rubbia, *Decoupling supernova and neutrino oscillation physics with LAr TPC detectors*, JCAP **0408** (2004) 001 [arXiv:hep-ph/0404151].

[9] A. G. Cocco, A. Ereditato, G. Fiorillo, G. Mangano and V. Pettorino, *Supernova relic neutrinos in liquid argon detectors*, JCAP **0412** (2004) 002 [arXiv:hep-ph/0408031].

[10] C. Rubbia, *The Liquid-Argon Time Projection Chamber:A New Concept For Neutrino Detector*, CERN-EP/77-08(1977).

[11] S. Amerio *et al.* [ICARUS Collaboration], *Design, construction and tests of the ICARUS T600 detector*, Nucl. Instrum. Meth. A **527** (2004) 329.

[12] F. Arneodo *et al.* [ICARUS-Milano Collaboration], *Performance of a liquid argon time projection chamber exposed to the WANF neutrino beam*, Phys. Rev. D **74** (2006) 112001 [arXiv:physics/0609205].

[13] B. Fleming, *LAr detector R&D in the US*, talk at NNN09, Estes Park, Oct. 2009.

[14] T. Maruyama, *LAr detector R&D in Japan*, talk at NNN09, Estes Park, Oct. 2009.

[15] E. Gatti *et al.*, *Considerations for the design of a time projection liquid argon ionization chamber*, IEEE Trans. Nucl. Sci. **26** (1979) 2910.

[16] D. Angeli *et al.*, *Towards a new Liquid Argon Imaging Chamber for the MODULAr project*, JINST **4** (2009) P02003.

[17] A. Breskin *et al.*, *A concise review on THGEM detectors*, Nucl. Instrum. Meth. A **598** (2009) 107 [arXiv:0807.2026 [physics.ins-det]].

[18] R. Alon *et al.*, *Operation of a thick gas electron multiplier (THGEM) in Ar, Xe and Ar-Xe*, JINST **3** (2008) P01005.

[19] P. Otyugova, *Development of a Large Electron Multiplier (LEM) based charge readout system for the ArDM experiment*, Diss. ETH No. 17704, 2008.

[20] A. Bondar, A. Buzulutskov, A. Grebenuk, D. Pavlyuchenko, Y. Tikhonov and A. Breskin, *Thick GEM versus thin GEM in two-phase argon avalanche detectors*, JINST **3** (2008) P07001 [arXiv:0805.2018 [physics.ins-det]].

[21] RD51 Collaboration, `http://rd51-public.web.cern.ch/RD51-Public/Welcome.html`

[22] A. Badertscher *et al.*, *Construction and operation of a Double Phase LAr Large Electron Multiplier Time Projection Chamber*, arXiv:0811.3384 [physics.ins-det].

[23] A. Badertscher *et al.*, *Operation of a double-phase pure argon Large Electron Multiplier Time Projection Chamber: comparison of single and double phase operation*, Nucl.Instr.andMeth.A(2009), doi:10.1016/j.nima.2009.10.011 [arXiv:0907.2944 [physics.ins-det]].

[24] A. Rubbia, *ArDM: A ton-scale liquid argon experiment for direct detection of dark matter in the universe*, J. Phys. Conf. Ser. **39** (2006) 129 [arXiv:hep-ph/0510320].

[25] S. Centro, *Cost effective electronics for LAr and photodetectors readout*, to appear in CERN Yellow Report - Future Neutrino Physics Workshop, CERN, October 2009

[26] C. Girerd *et al.*, *Cold front-end electronics and Ethernet-based DAQ system for large LAr TPC readout*, to appear in CERN Yellow Report - Future Neutrino Physics Workshop, CERN, October 2009

[27] P. K. Lightfoot, G. J. Barker, K. Mavrokoridis, Y. A. Ramachers and N. J. C. Spooner, *Optical readout tracking detector concept using secondary scintillation from liquid argon generated by a thick gas electron multiplier*, JINST **4** (2009) P04002 [arXiv:0812.2123 [physics.ins-det]].

[28] G.T. Mulholland, *LANNDD Feasibility Study*, Aug. 13, 2002, `http://www.hep.princeton.edu/~mcdonald/nufact/mulholland/ELAN_Proposal.pdf`

[29] Technodyne International Ltd, *Large Underground Argon Storage Tank Study report*, December 2004, commissioned by ETH Zurich.

[30] Géostock Group, `http://www.geostockgroup.com`

[31] W. Jaskierny, H. Jostlein, S. H. Pordes, P. A. Rapidis and T. Tope, *Test of purging a small tank with argon*, FERMILAB-TM-2384-E.

[32] L. Kaufmann and A. Rubbia, *The ArDM Project: A Direct Detection Experiment, Based On Liquid Argon, For The Search Of Dark Matter*, Nucl. Phys. Proc. Suppl. **173** (2007) 141.

[33] A. Curioni *et al.*, *A Regenerable Filter for Liquid Argon Purification*, Nucl. Instrum. Meth. A **605** (2009) 306 [arXiv:0903.2066 [physics.ins-det]].

[34] B. Baibussinov *et al.*, *Free electron lifetime achievements in Liquid Argon Imaging TPC*, arXiv:0910.5087 [physics.ins-det].

[35] R. Andrews, W. Jaskierny, H. Jostlein, C. Kendziora, S. Pordes and T. Tope, *A System To Test The Effects Of Materials On The Electron Drift Lifetime In Liquid Argon And Observations On The Effect Of Water*, Nucl. Instrum. Meth. A **608** (2009) 251.

[36] B. Rossi *et al.*, *A prototype liquid Argon Time Projection Chamber for the study of UV laser multi-photonic ionization*, JINST **4** (2009) P07011 [arXiv:0906.3437 [physics.ins-det]].

[37] Figure courtesy of F. Sergiampietri.

[38] A. Rubbia, *Neutrino factories: Detector concepts for studies of CP and T violation effects in neutrino oscillations*, arXiv:hep-ph/0106088.

[39] D. B. Cline, F. Sergiampietri, J. G. Learned and K. McDonald, *LANNDD: A massive liquid argon detector for proton decay, supernova and solar neutrino studies, and a neutrino factory detector*, Nucl. Instrum. Meth. A **503** (2003) 136 [arXiv:astro-ph/0105442].

[40] A. Ereditato and A. Rubbia, *Conceptual design of a scalable multi-kton superconducting magnetized liquid argon TPC*, Nucl. Phys. Proc. Suppl. **155** (2006) 233 [arXiv:hep-ph/0510131].

[41] A. Rubbia, *Underground Neutrino Detectors for Particle and Astroparticle Science: the Giant Liquid Argon Charge Imaging ExpeRiment (GLACIER)*, J. Phys. Conf. Ser. **171** (2009) 012020 [arXiv:0908.1286 [hep-ph]].

[42] D. B. Cline, F. Raffaelli and F. Sergiampietri, *LANNDD: A line of liquid argon TPC detectors scalable in mass from 200-tons to 100-ktons*, JINST **1** (2006) T09001 [arXiv:astro-ph/0604548].

[43] H. Chen *et al.* [MicroBooNE Collaboration], *Proposal for a New Experiment Using the Booster and NuMI Neutrino Beamlines: MicroBooNE*, FERMILAB-PROPOSAL-0974.

[44] D. Autiero *et al.*, *Test beam exposure of a Liquid Argon TPC Detector at the CERN SPS North Area*, Abstract #82, Workshop on New Opportunities in the Physics Landscape at CERN, May 2009

[45] The LAGUNA design study is financed by FP7 Research Infrastructure "Design Studies", Grant Agreement No. 212343 FP7-INFRA-2007-1. See `http://laguna.ethz.ch`

Large Water Cherenkov Detectors - Technical Issues -

H. Aihara
Department of Physics and IPMU
The University of Tokyo, Japan

Abstract
We address technical issues and challenges to construct a one-megaton scale water Cherenkov detector for neutrino detection. Studies presented here are mostly based on preliminary work for Hyper Kamiokande project.

1 Large Water Cherenkov Detectors

A large water Cherenkov detector with a total mass of about one megaton has been envisioned as a far detector for a next generation long baseline neutrino oscillation experiment as well as a fully active detector for a nucleon decay experiment. There are currently at least three independent proposals to construct such a detector: Hyper Kamiokande in Japan, Water Cherenkov detector(s) at DUSEL in US and MEMPHYS in Europe.

The current design of Hyper Kamiokande, shown in Fig. 1, calls for two identical large caverns, each containing a cylindrical detector of 43 m in diameter and 250 m in length. Each detector holds the amount of water corresponding to a fiducial volume of 540k ton and is instrumented with 50,000 20-inch Super-Kamiokande type phototubes. The total photo cathode coverage is 20% of the water surface. Its site is in Tochibora mine in Kamioka town in Japan and has overburden of 680 m..

Deep Underground Science and Engineering Laboratory (DUSEL) at Homestake in USA is a multi-disciplinary lab to address the underground needs of all the major scientific fields. There is a proposal to build three water Cherenkov detectors, each having a fiducial volume of 100k ton, at the site 4850 feets below the ground as shown in Fig. 2. It has 1455 m worth overburden. US neutrino physicists are pursuing to build these detectors as far detectors for a long baseline neutrino experiment using neutrinos produced at Fermilab.

A European project, MEMPHYS (MEgaton Mass PHYSics), is to build three large cylindrical (65 m diameter $\times$ 65 m high) water Cherenkov detectors (Fig. 3). The total fiducial mass of three detectors amounts to 440k ton. Each detector will be instrumented with 81,000 12-inch phototubes, providing 30% photocathode coverage of the water surface. It is envisioned to site in Frejus tunnel and the site has 4800 m water equivalent overburden.

2 Large Cavern Engineering

The issues related to excavating large caverns are specific to the candidate site that houses the proposed large Water detectors. For example, Finite Element Analysis has been done for Hyper Kamiokande site. Because the cavern is so large (48 m wide $\times$ 54 m high $\times$ 250 m long) cavern displacement and stability are of critical concern. The study showed that North-South cavern direction results in the smaller displacement ($\sim$ 55mm) of the cavern wall than East-West. Required are further site evaluation including global geological mapping (rock composition and position of faults), and in-situ rock mass properties (3D initial stress, Modulus of deformability and Young's modulus). Exploratory drilling is scheduled prior to finalizing the caver design.

R&D issues on excavation method include development of speedy and cost-effective method, design of main haulage tunnels, and disposal (or reuse) of excavated waste rocks. These are strongly coupled with environmental assessment and have a significant impact on the construction schedule.

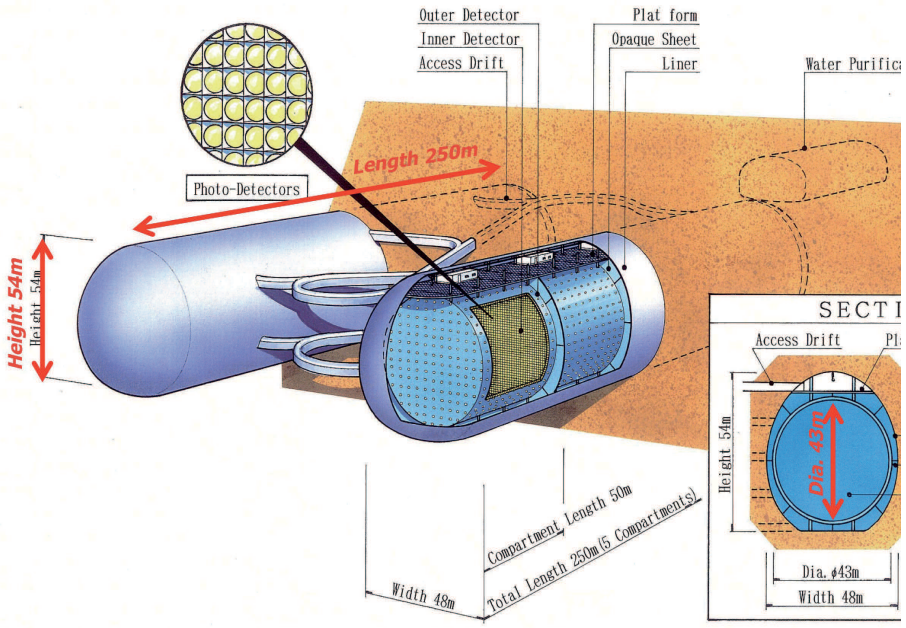

Fig. 1: Hyper Kamiokande, a megaton water Cherenkov detector, is proposed as a successor to Super Kamiokande, to be located at Tochibora, a few kilometers from the Kamioka site.

3 Tank and Water

Different types of tank wall (i.e. liner) material have been considered. They include self supporting steel can, segmented concrete blocks, self supporting concrete vessel, self formed concrete from top or bottom, and no liner (i.e. water barrier over shotcrete). Hyper Kamiokande plans to use plastic (high density polyethylene) liner, which is commonly used for public dump/landfill sites to protect environment from being polluted.

The choice of liner material imposes severe constraint on the performance of a water purification system. Water in Super Kamiokande, which has stainless steel liner, must be continuously purified. It was also the case for IMB (plastic liner) and SNO (acrylic liner).

The current baseline design of Hyper Kamiokande has 5 segmentation walls in a water tank. These walls define 5 sensitive compartments within a tank and also serve as a support structure of phototubes.

4 Photosensors and Electronics

These items are cost drivers as well as a schedule driver. A study for DUSEL shows that the total project cost breaks down to 30% for cavern construction and 70% for instrumentation. The instrumentation cost is driven by the price of photosensors and the associated electronics. The baseline design of Hyper Kamiokande deploys 100,000 20-inch Super-Kamiokande type phototubes to cover 20% of water surface with photocathode. The total cost of phototubes plus protective covers amounts to ∼$350M and that of associated electronics ∼$30M.

The cost reduction has been considered; 1) simply to reduce the photocathode coverage from 40% (of Super Kamiokande) to 20%, 2) to develop phototubes with higher quantum efficiency allowing fewer phototubes for the same photon collection, and finally 3) to develop a new photosensor whose price is lower than a phototube.

Other issues related to instrumentation are optimization of the aperture of phototubes (20 inch or smaller), optimization of the readout electronics in general, and design of protective covers or improving

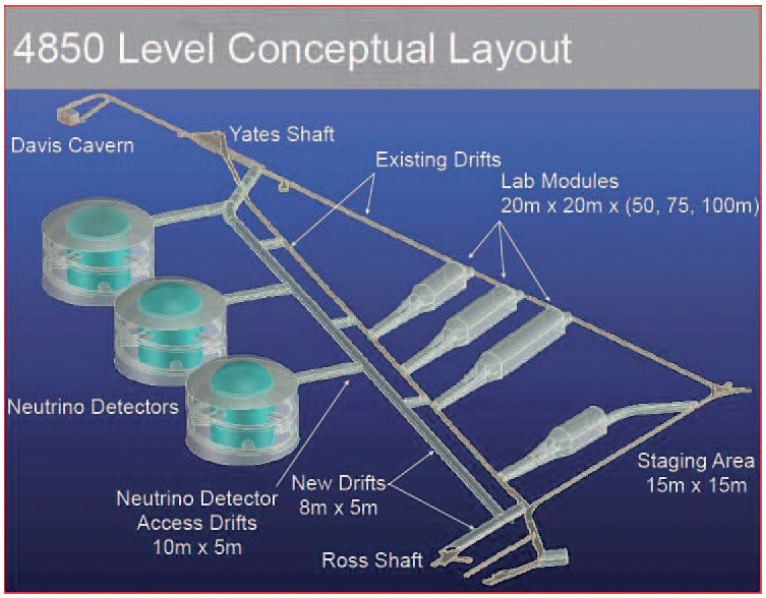

Fig. 2: Three 100k ton fiducial water Cherenkov detectors proposed for the Deep Underground Science and Engineering Lab (DUSEL) at Homestake

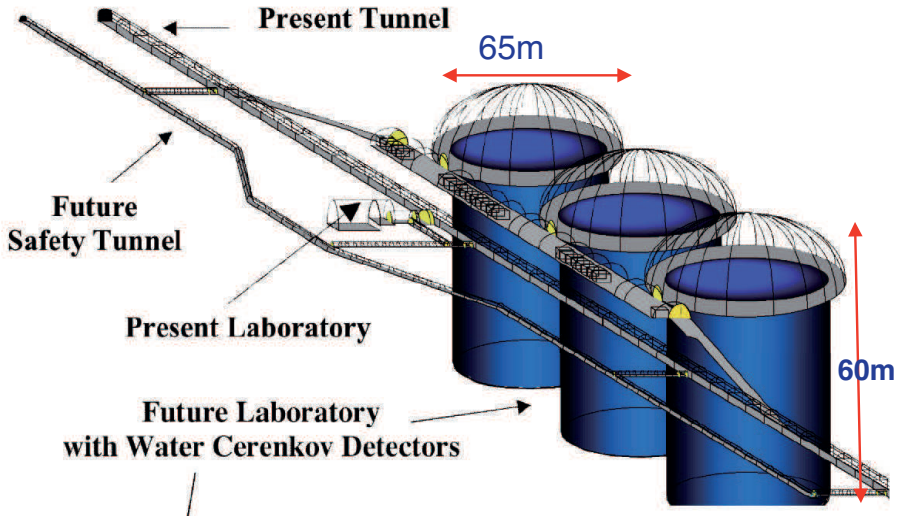

Fig. 3: MEMPHYS (MEgaton Mass PHYSics), proposed for the Frejus site, consists of three large cylindrical (65m diameter $\times$ 65m high) water Cherenkov detectors.

pressure-resistance of phototubes.

4.1 Photocathode coverage

Photocathode coverage is one the most critical parameters when designing a large water Cherenkov detector. There exist a few experimental proofs to show a reduced coverage of 20% will just do the job as well as the coverage of 40%. Super-Kamiokande collaboration reported a preliminary study on search for proton decay through $p \rightarrow \bar{\nu} K^+$ using data from SK-II data taking period and compared with the published result from SK-I data. SK-II data represents the photocathode coverage of 20% while the

original SK-I data 40%. In this analysis it is a key to identify a faint π^+ signal from $K^+ \to \pi^0\pi^+$. In SK-I data a typical number of photoelectrons from π^+ is about 60 and the analysis then required a π^+ signal have a number of photoelectrons between 40 and 100, while the corresponding number for SK-II data is from 20 to 50. Figure 4 shows the forward-backward display of $p \to \bar{\nu}K^+ \to \bar{\nu}\pi^0\pi^+$ simulation event for SK-I (the photocathode coverage of 40%). In the end, Super-Kamiokande collaboration finds the overall detection efficiency of $p \to \bar{\nu}K^+ \to \bar{\nu}\pi^0\pi^+$ for SK-II ($\epsilon \sim 4.8\%$) is about 80% of that for SK-I ($\epsilon \sim 6.2\%$) and the amount of background is comparable.

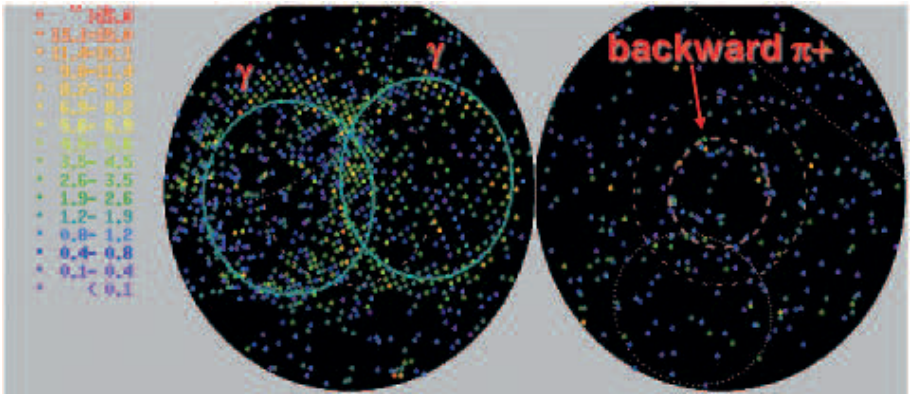

Fig. 4: Forward-backward display of $p \to \bar{\nu}K^+ \to \bar{\nu}\pi^0\pi^+$ simulation event for SK-I whose photocathode coverage is 40%.

Another example is Super-Kamiokande results of $p \to e^+\pi^0$ and $p \to \mu^+\pi^0$ search [1]. They have found almost identical detection efficiencies for SK-I and SK-II data, $\epsilon \sim 44\%$ for $p \to e^+\pi^0$ and $\epsilon \sim 35\%$ for $p \to \mu^+\pi^0$.

In addition, under study is whether the sensitivity to CP violation in a long baseline neutrino oscillation experiment degrades or not due to the reduced photocathode coverage.

4.2 High quantum efficiency phototubes

Hamamatsu Photonics (HPK) recently announced a new phototube whose quantum efficiency (QE) exceeds 42% at wavelength of 350 nanometers [2]. The QE of this device is about 1.7 times higher than that of the currently popular phototube as shown in Fig. 5. The increase in Q.E. compensates the loss of the photocathode coverage.

4.3 A new photosensor

A large aperture Hybrid Avalanche Photodetector (HAPD) has been developed. Figure 6 illustrates the structure of HAPD. HAPD accelerates photoelectrons by a high voltage (ranging from 10 to 20 kV) applied between a photocathode and an avalanche diode (AD) to bombard them into AD. Each photoelectron generates secondary electrons ($\sim$ 5000 electrons at 20 kV) and they, in turn, go through avalanche multiplication of $\sim 30 - 50$. This two-stage multiplication results in a total gain of $\sim 10^5$ for each photoelectron. HAPD has several advantages over a phototube with dynodes. The large first gain (i.e. bombardment gain) reduces an output pulse height fluctuation. HAPD is, therefore, expected to have better pulse height resolution than a phototube. HAPD does not have dynodes that introduce variation in transit time of secondary electrons. HAPD is expected to have smaller transit time spread (TTS). Power consumption of HAPD is also less because there is no dynode current. Because HAPD has fewer components than a phototube (AD vs dynodes), it is also expected to be less expensive.

A 13-inch HAPD shown in Fig. 7 has been developed by HPK, the University of Tokyo and

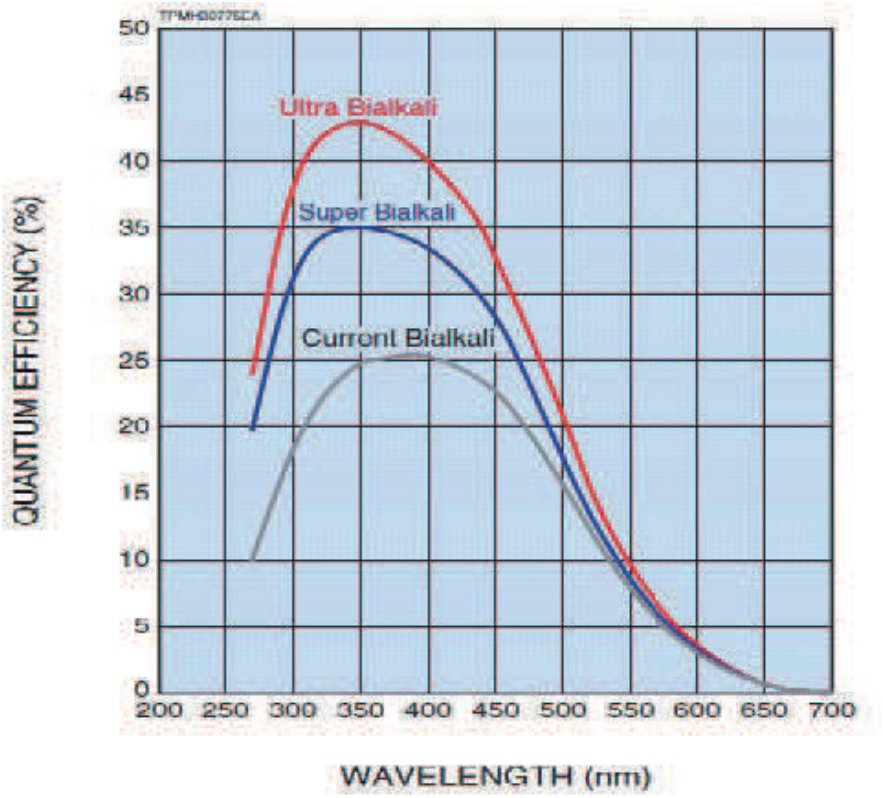

Fig. 5: Quantum Efficiency (QE) of ultra and super bialkali photocathodes. QE of ultra bialkali reaches 43% at 380nm, a factor of ~ 1.7 improvement over the conventional one.

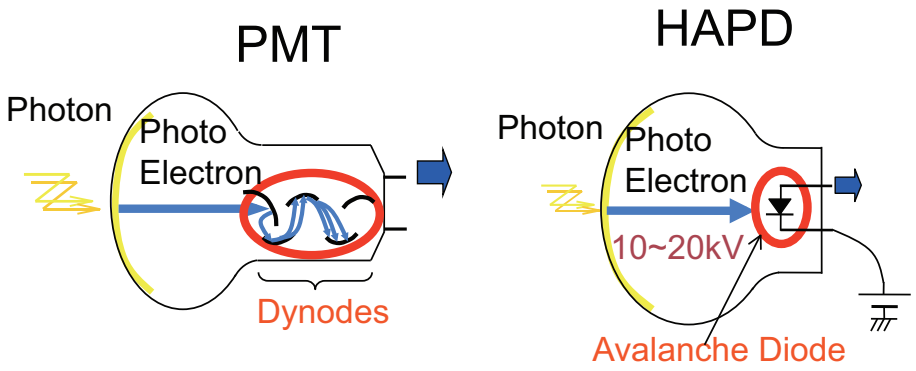

Fig. 6: Schematic presentaion of operation principles of phototubes (PMTs) and Hybrid Avalanche Photodetectors (HAPDs).

KEK [3]. A compact digital readout electronics based on waveform sampling has also been developed. Table 1 summarizes its performance compared with that of phototubes. Large aperture (13 and 8-inch) HAPDs are expected to be commercially available from HPK by 2013.

In Europe a project called PMm^2 [4] has been launched to develop large photomultipliers and innovative electronics for the next-generation neutrino experiments. The very large surface of photodetection is segmented in macro pixels made of 16 hemispherical (12-inch) photomultiplier tubes connected to an autonomous front-end which works on a triggerless data acquisition mode. The expected data transmis-

Table 1: Summary of HAPD performance compared with that of phototubes. All devices are HPK products.

	13-inch HAPD	**13-inch PMT** (R8055)	**20-inch PMT** (SK type)
single photon time resolution (TTS)	190 ps	1400 ps	2300 ps
single photon pulse height resolution	24%	70%	150%
Quantum efficiency	20%	20%	20%
Electron collection efficiency	97%	70%	70%
Power consumption	$<<$ 700 mW	$\sim$ 700 mW	$\sim$ 700 mW
Total gain	10^5	10^7	10^7

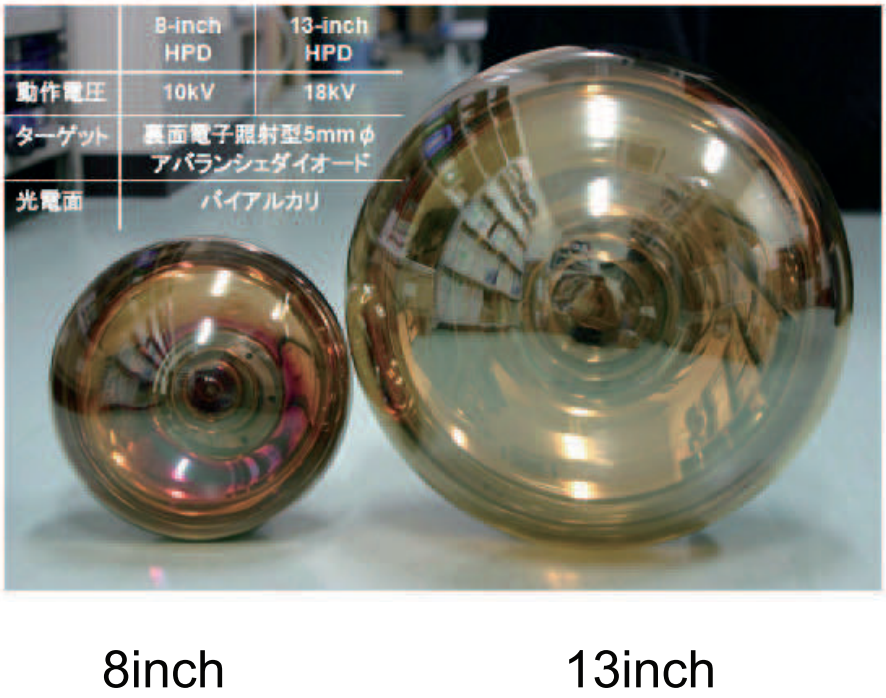

Fig. 7: Large aperture HAPDs soon to be commercially available.

sion rate is 5 Mb/s per cable, which can be achieved with existing techniques. Figure 8 illustrates the architecture.This architecture allows reducing considerably the cost and facilitating the industrialization.

5 Conclusion

We have presented a snapshot of on-going R&D of large water Cherenkov detectors for neutrino physics. Although there are still many technical issues ahead of us, we conclude that it is certainly feasible to construct such a large detector or detectors based on the experience gained by its predecessors such as Super Kamiokande. The instrumentation of photosensors is the major cost driver and the efforts to reduce its cost is underway. The construction of such a large water Cherenkov detector is estimated to take 7 to 10 years. It is generally agreed among those who have worked on a large water Cherenkov detector that it is not necessary to take the intermediate steps before we embark on a full-scale construction.

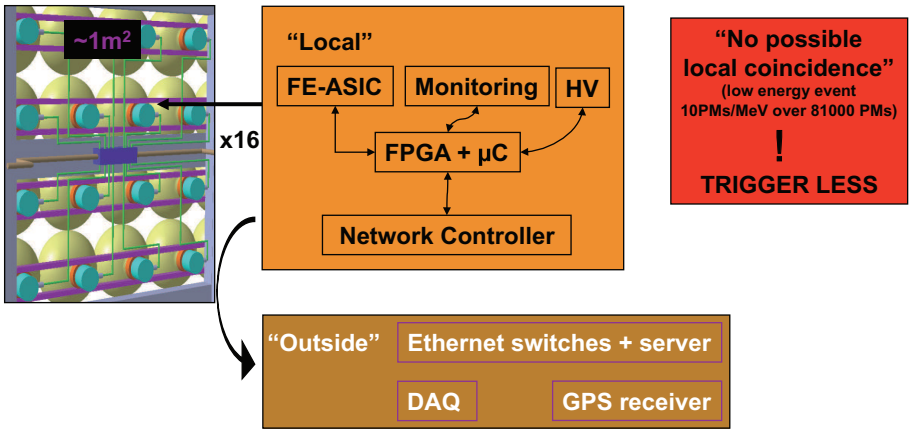

Fig. 8: The signal readout architecture developed by PMm^2 project for large water Cherenkov detectors.

Acknowledgements

We wish to thank the organizers of the workshop and, in particular, Professor Alain Blondel for his effort to edit the proceedings and his patience.

References

[1] H. Nishino *et al.*, (Super-Kamiokande Collaboration), Phys. Rev. Lett. **102**:141801, 2009.
[2] M. Suyama and K. Nakamura, Proceedings of Science, PoS(PD09)013.
[3] T. Abe *et al.*, Proceedings of Science, PoS(PD09)014.
[4] B. Genolini *et al.*, Nucl. Instrum. Meth. **A610**, 249-252, 2009.

Underground Facilities, Technological Challenges

Neil Spooner
University of Sheffield

Abstract
This report gives a summary overview of the status of international underground facilities, in particular as relevant to long-baseline neutrino physics and neutrino astrophysics. The emphasis is on the technical feasibility aspects of creating the large underground infrastructures that will be needed in the future to house the necessary detectors of 100 kton to 1000 kton scale. There is great potential in Europe to build such a facility, both from the technical point of view and because Europe has a large concentration of the necessary engineering and geophysics expertise. The new LAGUNA collaboration has made rapid progress in determining the feasibility for a European site for such a large detector. It is becoming clear in fact that several locations are technically feasible in Europe. Combining this with the possibility of a new neutrino beam from CERN suggests a great opportunity for Europe to become the leading centre of neutrino studies, combining both neutrino astrophysics and neutrino beam studies.

1 Introduction - Requirements and Challenges

There has been increased scientific motivation in recent years to consider construction of a very large underground detector of scale 100-1000 ktons that can approach simultaneously several key scientific questions across a range of particle astrophysics and high energy physics. Notable here is the drive to improve limits on proton decay by at least $\times 10$, particularly for the kaon channel; to measure the flux of background neutrinos predicted from past supernova; to observe with great precision the neutrino flux and spectra from any nearby supernova explosion; to observe geo-neutrinos from the Earth, (a new field that promises to unravel the radio-chemical composition of the Earth that is poorly understood); to study solar neutrinos with great precision, and finally to detect dark matter via neutrinos from annihilation of neutralinos in the Sun or Galaxy. These topics provide the main aims of such a detector. However, such a device would also be a natural target for neutrinos from a possible nearby reactor or eventually a future neutrino beam, opening in particular exciting prospects for studying CP violation and hence to understand the origin of the matter-antimatter asymmetry.

The prospect for building such a detector with this impressive range of science goals is stimulated further by rapid technological advances that make its feasibility much more plausible than appeared possible only 10 years ago. For instance, our understanding of constructing large infrastructures underground has improved, stimulated by a rapid growth in underground science interests as a whole but also commercial reasons for underground engineering. The development at Homestake mine in the US of the Deep Underground Science and Engineering Laboratory (DUSEL) concept is an example. Other current underground laboratories have also undergone recent extensions, including at Kamioka (Japan), SNOlab (Canada) and elsewhere. In Europe, there have also been significant extensions to existing underground infrastructures, for instance at Canfranc (Spain) and Boulby (UK), with advanced plans at Frejus (France) and elsewhere. Boosted by the European funded ILIAS (Integrated Large Infrastructures for Astroparticle Science) programme the four current deep science laboratories in Europe, comprising Boulby, Canfranc, Frejus and Gran Sasso (Italy), have become more closely integrated, allowing greater pooling of knowledge, expertise and resources. This general picture places Europe in a strong position to lead future large underground facility construction.

Meanwhile, there has also been rapid development in detector technology that points the way to building the necessary next-generation large neutrino detectors themselves. Notable is the success of the Borexino solar neutrino experiment at Gran Sasso. This has demonstrated the feasibility of operating large volumes of liquid scintillator (100's tons) with radio-purity at the 10^{-18} part of U level. Large volume liquid argon technology is also maturing, with many groups developing new concepts, building on the first generation of ICARUS. For water Cherenkov technology, the experiences with SuperK at Kamioka and development of large area, low cost, photomultiplier tubes, also point to the feasibility of scale-up towards a megaton. These advances have been crystallised in Europe into three detector concepts for the next generation of large detector, notably LENA (a massive liquid scintillator concept of $\sim$50 ktons), MEMPHYS (a massive water Cherenkov detector of $\sim$300 ktons) and GLACIER (a concept using $\sim$100 ktons of liquid argon) [1]. Nevertheless, there are clearly major challenges for such an ambitious project. Some of the questions that need addressing are, for instance:

- Which of these technologies can provide the best physics value: scintillator, Cherenkov or argon?
- How can the necessary tank infrastructure be engineered underground?
- What geographic location is best for the site, taking into account both geophysics arguments and physics needs such as the baseline to a potential neutrino beam?
- How should the necessary large caverns (of order 70 m scale) be excavated deep underground?
- What are the socio-economic, environmental and legal or planning issues involved in building and running such a large underground laboratory?

In Europe the LENA, MEMPHYS and GLACIER collaborations are now united within the context of the LAGUNA (Large Apparatus for Grand Unification and Neutrino Astrophysics) programme funded by the EU as a design study to compare together potential underground sites, in the context of the detector options [2]. The detector developments themselves are at different stages of technical maturity and offer different, somewhat complementary, potential science reach. There are differences in the challenges these options face to achieve the necessary detector volumes. For instance, for the GLACIER concept new techniques are needed to handle large quantities of cryogenic liquid and the high voltages required for the drift field. However, the detectors also share many common features. Foremost among these is the requirement for a large containment tank and for construction of a cavern (or caverns) of volume up to 10^6 m^3 that need to be located deep (500-1500m) underground and survive for at least 30 years.

In fact tank technology is quite well understood, thanks to the liquid petroleum gas industry, where construction of tanks with volumes even larger than required for LAGUNA are routinely unertaken. However, to date there exists no direct experience of excavating such large caverns at depth. The report here aims to summarise this aspect of the field, the progress and state of knowledge for large cavern infrastructure. Detailed discussion of detector options and progress is covered elsewhere in this volume.

2 Status of World Underground Science Site Expansion

Table 1 gives summary information on the status of most of the better known current deep underground science facilities in the world. Although many of these are engaged in expansion plans, for instance there is the ULISSE project at Frejus, the new cryolabs at SNOlab and new laboratories at Kamioka, these efforts are aimed at medium scale experiments, mainly for next-generation dark matters searches and double beta decay experiments. Actually, most current sites are, for various reasons, deemed unsuitable for very large caverns. This includes Gran Sasso in Italy, currently the world's largest, where any substantial expansion is likely ruled-out for environmental reasons. At SNOlab also, currently the world's deepest significant facility, expansion to the required scale looks unfeasible for logistical reasons (rock removal capacity). Instead there is growing activity directed at the feasibility of new sites.

Outside Europe, in Asia and North America, we can highlight four potential sites. In Southern India at Masinagudi in the Nilgiri area, serious studies are underway for the Indian Neutrino Observatory

(INO) at a new site at 1300m depth with horizontal access [3]. The prime aim here is for a 50 kT magnetized iron detector. The Nilgiri massif is known to comprise highly compacted granite which is more suitable for tunneling deep underground caverns than locations in the Himalayas. There is an exciting new development also in central China near the Yalong river in the Jinping mountain region [4]. This is set to provide a new facility with rock overburden $\sim$2500m, deeper than SNOlab but with horizontal road access. So far a small test cavity of 5x5x30m has been built there for evaluation, prior to establishment of a new Chinese Deep Underground Laboratory (CDUL) in the next decade.

The new sites above have future potential for large neutrino detectors but currently closer to this goal are the efforts at DUSEL (USA) and in Japan. For the latter several sites have been considered for a megaton scale detector (either water Cherenkov or liquid argon) to supersede SuperK in association with a neutrino beam from JPARC. One candidate site is at the Toshibara mine at a depth of $\sim$600m close to the SuperK site. Here, bore-holes and in-situ rock stress studies are well advanced, determining a preferred design for a Cherenkov experiment (HyperK) comprising two horizontal tanks oriented North-South, to cope with the local rock jointing. This site provides a baseline from JPARC of $\sim$295km. However, other sites are under study at Okinoshima island in Japan (658km) and in S. Korea ($\sim$1000km).

A large water Cherenkov array or liquid argon experiment at the proposed Deep Underground Science and Engineering Laboratory at Homestake, South Dakota, is being considered as a flag-ship experiment for this new US site. The base-line design here envisages multiple 100 kton scale caverns suitable for vertical cylindrical tanks at the 4850 ft level in stable amphibolites rock. Geological mapping is underway with exploratory bore holes and drift tunnels planned soon. This site would have a baseline of 1300 km from a Fermilab neutrino beam.

3 European Sites and LAGUNA

Turning to Europe, the focus here has been the LAGUNA collaboration (Large Apparatus for Grand Unification and Neutrino Astrophysics), funded as a 2 year design study from late 2008 under the EU FP7 programme, to consider the feasibility of building a new large neutrino detector infrastructure deep underground in Europe. LAGUNA is a highly interdisciplinary consortium, linking European physicists interested in massive neutrino detectors with geo-technical experts, geo-physicists, structural engineers, tank and mining engineers. There are 21 beneficiary organisations, including 9 (+4 associate) HE institutes, 8 other research organisations and 4 companies from across 9 countries. Work is divided into three workpackages plus management, comprising: (i) Underground Infrastructure and Engineering; (ii) Safety, Environment and Socio-Economic aspects, and (iii) Science Impact and Outreach. The main emphasis is on the geo-technical and engineering feasibility of a large underground site. However, the importance of environmental issues, the economic and societal impact and influence (positive or negative) on the local and national host region, and the need for the highest safety standards, is also well recognised, hence the second workpackage above.

After an early period of consultation, LAGUNA was formed with 7 pre-selected underground sites in Europe, to be studied in relation to 3 detector technologies: GLACIER (liquid argon), LENA (liquid scintillator) and MEMPHYS (liquid water), with all groups working together on common areas. A clear timetable has been developed that fits well both with the need to construct LAGUNA to achieve the well known core particle astrophysics science goals (see Section 1) on a competitive timescale, and the prospects of adding further physics reach with a neutrino beam at a latter stage, for instance compatible with a new beam from CERN in 10 years time. This calls for an initial site/detector prioritization and down-select (July 2010), a more focussed (LAGUNA-NEXT) design and study (2011-2012), a detailed construction phase study (2012-2015), then full construction from 2015.

The seven pre-selected LAGUNA locations (listed here with their distance to CERN) comprise 4 sites in existing working mines: Boulby, UK (1050 km); Pyhasalmi, Finland (2300 km); Sieroszwice/ SUNLAB, Poland (950 km) and SLANIC, Romania (1200 km); plus 3 tunnel sites: Canfranc, Spain

Table 1: Summary characteristics of the world's deep underground laboratories

Site	Location and access	Current space	Depth and muon flux (μ $m^2 s^1$)	Rock and radon (Bq m^{-3})
Europe				
BNO	Andyrchi, Russia; independent tunnel	3 halls: 24×24×16 m^3; 60×10×12m^3; 40,000 m^3	850 m.w.e. and 4700 m.w.e. (SAGE area); 3.03±0.19×10^{-5}	40 norite rock
BUL	Boulby mine, UK; vertical	1,500 m^2	2800 m.w.e. under flat surface; 4.5±0.1×10^{-4}	1-5 salt
CUPP	Pyhasalmi mine, Finland; vertical	>1000 m^2 spaces no longer used by the mine	down to 1400 m	- pyrite ore, zinc ore
LNGS	Gran Sasso, Italy; road tunnel	3 halls plus tunnels total 17,300 m^2; 180,000 m^3	3200 m.w.e., under mountain; 3×10^{-4}	50-120 $CaCO_3$ and $MgCO_3$
LSC	Canfranc, Spain; road tunnel	2 halls: 40×15×12m^3; 15×10×8m^3; tot 1000m^2	2400 m.w.e., under mountain; 2×10^{-3} - 4×10^{-3}	50-80 limestone
LSM	Modane, France; road tunnel	1 hall and service areas: 400 m^2	4800 m.w.e. under mountain; 4.7×10^{-5}	15; (0.01 filtered) calcitic schists
SLANIC	Prahova mine, Romania; vertical	70,000 m^2 average ht. 52-57 m	208 m, under flat surface	6 salt
SUNLAB	Sieroszowice mine, Poland; vertical	85×15×20 m^3	900-950 m (2200 m.w.e.) 650-700 m for large caverns	20 salt and copper ore
SUL (UK)	Solotwina mine, Ukraine; vertical	25×18×8 m^3; 4 of 6×6×3 m^3; total area 1000 m^2	1000 m.w.e. under flat surface; 1.7×10^{-2}	33 salt
Asia				
INO (proposed)	Masinagudi, India; independent tunnel	2 halls: 26×135×25 m^3; 53×12×9 m^3	3500 m.w.e.	- compacted granite
Kamioka	Japan; independent horizontal	Hall SK 50 m dia; 40×4 & 100×4 m with L-arm	2700 m.w.e. 3×10^{-3}	20-60 lead and zinc ore
Oto-cosmo	Tentsuji, Japan; Indep. horizontal	2 halls: 50 m^2; 33 m^2; total ∼100 m^2	1400 m.w.e. 4×10^{-3}	10 (radon reduced) -
Y2L	YangYang, S. Korea; horizontal	Current space: 100 m^2 Planned space: 800 m^2	∼2000 m.w.e. 2.7×10^{-3}	40-150 -
North America				
DUSEL (proposed)	Homestake, USA; vertical	7200, 4500, 100 m^2 at 1450, 2200, 2438 m dep	233, 4100, 6400, 7000 m.w.e. under flat surface	∼40-200 (at 1478 m) metasedimentary
SNOLAB	Creighton mine, Canada; vertical	SNO ∼200 m^2; main 18×15×15-19.5 m^2 ; ladders 6-7 m; total 46,648 m^2	6001 m.w.e. under flat surface 3×10^{-6}	120; norite, granite gabbro
SUL (US)	Soudan mine, USA; ∼vertical	2 halls: 72×14×14 m; 82×16×14 m; tot 2300 m^2	2000 m.w.e under flat surface 2×10^{-3}	300-700; Ely greenstone
WIPP	Carlsbad, USA; vertical	500×8×6 m available	2000 m.w.e. 2×10^{-3} expected	< 7; salt
Kimballton	Butt Mountain, USA; horizontal	30×11×6 m	1400 m.w.e	- Paleozoic dolomite

(630 km); Frejus, France (130 km); and Umbria, Italy (655 km). Of these only the Umbria site is a greenfield location with no previous excavation, chosen here for the quality of the rock, position along the CNGS beam and as an alternative to expansion of Gran Sasso which is currently ruled out. Umbria is considering the GLACIER detector concept as a priority. The SLANIC site has pre-existing salt caverns of size already sufficient in principle for the GLACIER concept. However, the relatively shallow depth (200-300m) is sufficient to rule out LENA and MEMPHYS options (and possibly also GLACIER without new, deeper excavations). The other sites are able the consider all detector options. Of the seven sites Boulby (mine), Canfranc (tunnel) and Frejus (tunnel) have significant previous experience of operating science infrastructure underground.

The LAGUNA team, through a series of 16 detailed deliverables backed by joint site visits and technical reports, aims to address all the key questions necessary to make a critical assessment of the strengths and weaknesses of each site, hence to produce a site prioritisation and eventual site/detector selection. Topics to be addressed include: the rock mechanics of the caverns, the design of tanks in relation to each site, the overburden in relation to detector physics, transport, access and liquid delivery issues, safety, environmental and rock removal issues, and relative costs. Impressive progress has been made in all these areas in the last two years. We outline here a few, necessarily selected, examples (further details and reports can be found at [2]):

3.1 Tank Concept

Detailed work on the design of the underground tank structures has been completed by Technodyne Ltd. and partners. This covers each detector concept and includes, in particular, the special requirements for underground fabrication and safety and, in the case of water and liquid scintillator, concepts in which the tank walls are integral to the cavern rock wall. The dimensions considered focus on a 65 m diameter cylinder by 70 m height (including dome roof) for MEMPHYs, 30 m diameter by 105 m height for LENA and 75 m diameter by 26.5 m height for GLACIER. Figure 1 shows an example for the GLACIER design. Here there is special consideration for suspension of the readout deck above the liquid. Underground fabrication allows for the possibility of fixing a construction crane to the roof of the cavern.

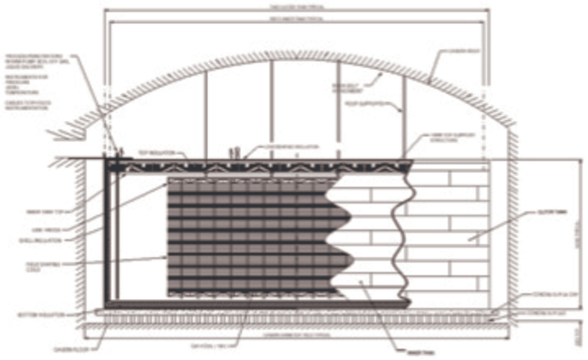

Fig. 1: Diagram of the GLACIER tank design

3.2 Geo-mechanical Studies

A core activity of LAGUNA is extensive geo-mechanical studies of the integrity and lifetime (both during and post construction) of the large excavations needed at each site. This has now been completed in preliminary form for all locations, using mainly FLAC3D and ABAQUS/CAE simulation software to determine the rock stress fields, convergence, spalling and requirement for rock-bolting. The work uses sets of known rock parameters at each site, obtained from existing bore holes, new samples acquired for

the project or from previous excavations. Figures 2(a) and 2(b) show example outputs for the SUNLAB and Boulby cases. To date no site has reported major concerns on the geo-mechanical feasibility. However, further rock parameter data is required at some sites and further study is needed on the influence of rock layering and jointing. Work is underway to make a critical comparison of the techniques and data used.

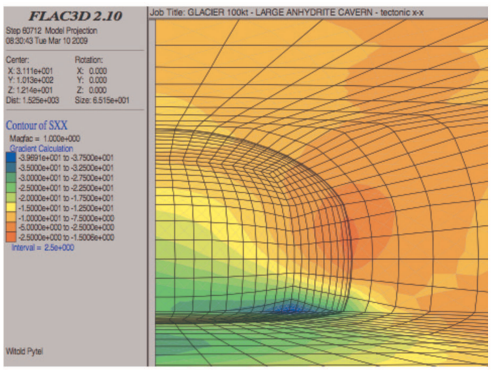

(a) Examples of σxx and σzz contours for MDC (GLACIER) at SUNLAB in anhydrite (depth 617.5 m; cavern subjected to tectonic stress) produced using FLAC3D

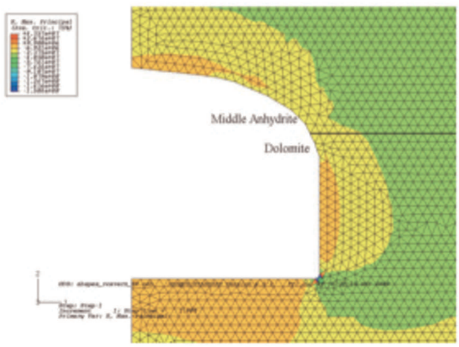

(b) Examples of maximum principle stresses around a GLACIER cavern in the anhydrite/dolomite layer at Boulby produced using ABAQUS

Fig. 2: Examples of geomechanical rock simulations

3.3 Main Cavern Engineering

Linking the two parts above is work on the Main Detector Cavern (MDC). Here the focus is on design of the MDC in relation to the detector, involving cooperation between tank engineers (Technodyne Ltd.) and mining/tunnelling engineers (e.g. Rockplan, Cuprun, CPL and AGT). Figure 3 Shows an example of the conceptual design for GLACIER at Umbria. Note here, as with other sites, the use of a concave floor excavation, necessary to reduce rock stress at the caverns corners, and entailing need for extensive concrete pillars to support the detector.

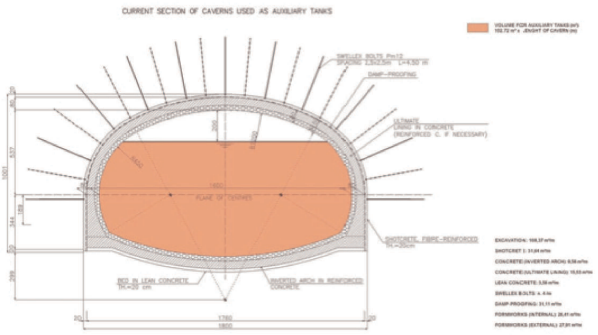

Fig. 3: Example Main Cavern Engineering design for GLACIER at Umbria

3.4 Layout Studies

With MDC studies well advanced, work has also been completed on details of layout of ancillary tunnels and access/egress routes at each site. Here, consideration of safety features, including evacuation routes and safe haven rooms, are vital, noting the different features required for road tunnel sites, where the general public are close by, compared to mine sites. Figure 4 Shows an example schematic layout for the LENA detector option at the Phyasalmi site. Double roadways are used to provide redundancy and for ventilation flow. Here, spiral roadways external to the MDCs are used to access these during excavation. Preliminary layouts for all sites have been completed. Figure 5 shows one design for a tank sited in the existing caverns at SLANIC.

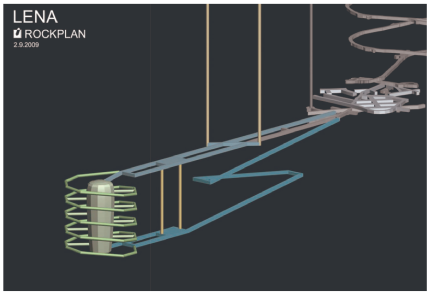

Fig. 4: Example schematic layout design for the LENA detector option at the Phyasalmi site

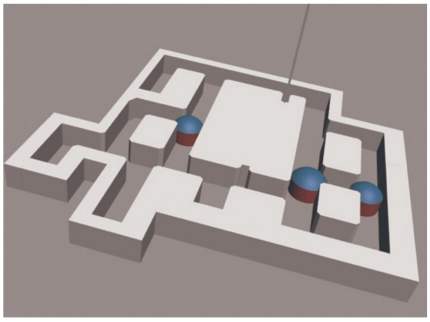

Fig. 5: Example layout design for tank sited in the existing caverns at SLANIC, Romania

3.5 Construction Sequencing

The process of construction and excavation has been studied not just from the geo-technical viewpoint but also addressing the logistics of rock removal and disposal. This is particularly important for the tunnel sites for which, unlike the mine sites, there is no existing infrastructure to help minimise the environmental hazard of rock disposal. For instance, for the greenfield site in Umbria, close collaboration has been needed with the Regional Environmental Agency (ARPA Umbria). Figure 6 Shows an example of the construction sequence for the Sieroszowice site, using a top-down excavation from the dome and including rock-bolting. At each site FLSAC3D or ABAQUS simulations have been used to ensure integrity at each stage of excavation and whether additional support is needed. For instance, the Canfranc site has considered an additional MDC roof excavation process that includes adding strength via backfilling roof tunnels with concrete.

3.6 Additional Infrastructure

All the detector options require further ancillary support laboratories and storage caverns. So the design of these has also been considered at all sites. This includes experiment control rooms, clean rooms, electronics and mechanical workshops but also any ancillary caverns needed for the construction phase and

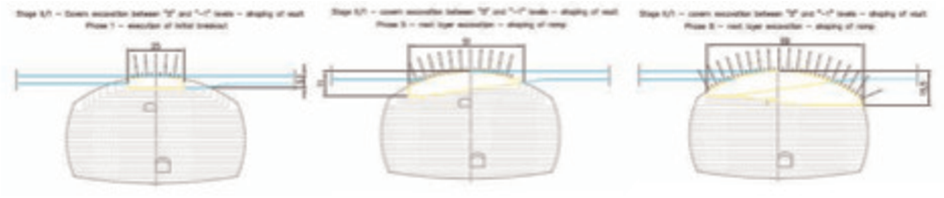

Fig. 6: Part of the construction sequence for the Sieroszowice site, using a top-down excavation from the dome and including rock-bolting

for emergency dump of liquids. In most cases the ancillary rooms can be located in cross-cut excavations (for instance at Phyasalmi, see Figure 4). Liquid dump and storage rooms require special consideration. Figure 7 shows an example concept for the Boulby site, using a gravity fed system.

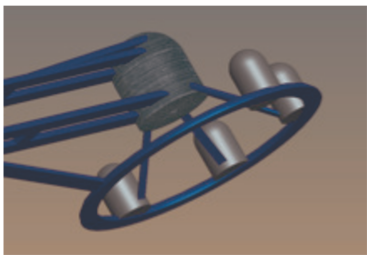

Fig. 7: Example concept liquid dump infrastructure for the Boulby site, using a gravity fed system

3.7 Socio-economic, Safety and Environment

The importance of these issues, failure in any of which could prevent construction even if feasible from the purely technical perspective, is recognised by all the sites. Hence, each has undertaken a detailed preliminary safety and hazard assessment and risk analysis. Specific concerns addressed include: whether there are particular planning law or environmental issues that would prevent construction (for instance, due to massive rock disposal or transport issues); whether safety risks, such as to the general public in the case of road tunnels, can be sufficiently mitigated against; and whether there are particularly favourable, or unfavourable, local or national economic and societal impacts.

4 Conclusion

For LAGUNA and the prospects of a firm European large detector project, rapid progress means much of the technical fact gathering is well advanced towards making a decision on site prioritisation and detector choice. Some particular issues are outstanding, such as the procurement and delivery of liquids underground. Here there are further challenges, particularly for liquid argon. Nevertheless, no real show-stoppers have been identified and there is growing confidence that the construction timelines suggested can be met and be aligned well with a possible future neutrino beam from CERN later. Outside Europe the US and Japanese efforts are also well advanced and there are signs that other large facilities elsewhere, particularly in China and India, are emerging.

Acknowledgments

NJCS would like to acknowledge support form the EU FP7 project 212343.

References

[1] D. Autiero et al., Journal of Cosmology and Astroparticle Physics JCAP11 (2007) 011

[2] http://laguna.ethz.ch:8080/Plone/

[3] http://www.imsc.res.in/_ino

[4] http://physics.sjtu.edu.cn/iwdd09/

Photon-detectors R&D for future neutrino experiments

T. Nakaya
Kyoto University, Kyoto, Japan

Abstract
We review the recent developments of new photon-detectors available for the future neutrino experiments. A photon-detector with large photo-coverage is the key component of a giant Cherenkov detector which will be an essential part of the future long baseline neutrino oscillation experiment to explore the CP violation in the neutrino sector. A photon-detector with fine pixels is also the key component to build a finely segmented scintillator detectors for precision neutrino experiments. We review the large photon-detectors, fine-segmented photon-detectors and a few novel ideas of photon-detectors.

1 Introduction

Neutrino physics has fascinating progress in decades with the birth of neutrino astronomy and the discovery of neutrino oscillations and mass. A new type of neutrino detectors often opened the new windows for discoveries, such as an observation of the solar neutrinos by the Homestake chlorine experiment, the detection of supernova neutrinos by the Kamiokande experiment, the discovery of neutrino oscillation and mass by the Super-Kamiokande experiment, etc.. A development of new photon-detectors sometimes played an crucial role to make the experiments successful.

We review the recent developments of the new photon-detectors available for neutrino experiments. One type of photon-detectors is a big device which will be used for gigantic neutrino detectors, such as a Megaton Water Cherenkov detector, a Neutrino Telescope and a big Liquid Scintillator detector. The other type of photon-detectors is a compact device with fine multi-pixels which could be used for the high resolution neutrino detectors, such as the near detector in the long baseline neutrino oscillation experiments or the far detector with a good particle identification capability.

We summarize the photon-detectors reviewed in the paper in Table 1, where "Area", "Dark curr.", "QE", "PDE", "B-field", and "Exp." are the abbreviations of "photon-sensitive area", "dark current", "quantum efficiency", "photon detection efficiency", "operation in the magnetic field", and "experiments", respectively. The photon detectors listed in the top part are for large water Cherenkov and liquid scintillator detectors, the photon detectors in bottom are for fine-grained detectors. These photon-detectors are described in the following sections.

2 Photon-detectors for Large Water Cherenkov and Liquid Scintillator Detectors

2.1 Hamamatsu 20" PMT

The biggest photon-detector is Hamamatsu R3600-05, which is widely known as 20" PMT of the Super-Kamiokande experiment. The 20" PMT has the large photo-coverage up to $\sim$2000 cm^2 with a good timing resolution of 2$\sim$3 nsec and adequate quantum efficiency (QE) of $\sim$20 %. It is tolerant up to $\sim$6 atmosphere pressure. The 11,200 PMTs are operated under the water in Super-Kmaiokande for more than 10 years, which proofs the reliability of the device. A few disadvantages of the PMT are not inexpensiveness ($\sim$\$3/device) and the uneasy handling because of the size.

The PMT is one of the promising candidates photon-detectors for a future Megaton-size water Cherenkov detector, such as Hyper-Kamiokande [1]. However, because of the disadvantages, a development of the inexpensive big photon-detectors is desired.

Table 1: Summary of photon-detectors introduced in this article.

Device	Area (cm^2)	Gain	Noise or Dark curr.	QE or PDE (%)	B-field	Exp.	Commercial Availability
20" PMT	2000	10^7	$O(10k)$ Hz	$\sim$20	$\times$	Super-K	◯
High-QE PMT	$\sim$500	10^7	$O(5k)$ Hz	30$\sim$40	$\times$	IceCube	◯
13" HAPD	$\sim$800	10^5	$\sim$PMT	$>\sim$20	$\times$	R&D	△
Gas PMT	$\sim$900	10^6	$\sim$PMT	$\sim$20	OK	R&D	$\times$
LAPD					OK?	R&D	$\times$
MA-PMT	0.1×256	10^6	$<$ 1kHz	10$\sim$20	$\times$	many exp.	◯
MA-MCP-PMT	0.1×64	10^6	$<$ 1kHz	10$\sim$20	OK		◯
APD	0.2×32	$\sim$100	$< 3000e$	70$\sim$85	OK	NOνA	◯
PPD (MPPC, ..)	$\sim$0.1	10^6	$O(1M)$Hz	30$\sim$45	OK	T2K	◯
MC-HAPD	0.3×144	10^5	$\sim 1\mu$A	$\sim$20	OK	R&D	△

2.2 High-QE PMT

Hamamatsu Photonics develops the higher QE PMTs, of that photo-cathodes are named as "Ultra Bialkali (UBA)" and "Super Bialkali (SBA)". The UBA photo-cathode has QE as high as 43 %, and the SBA has QE of 35 %. There are many types of PMTs with UBA and SBA photo-cathodes commercially available and the products are found in the commercial catalog of Hamamatsu Photonics.

Recently, the Ice Cube experiment adopts the 10" SBA PMTs and they tested the performance of SBA. They find the good QE as similar as that shown in the catalog. They also find that the count rate of the dark noise is twice more than that of the standard 10" PMT as expected in the specification.

The successful developments of these high QE PMTs are good news for the design of the future gigantic neutrino detectors.

2.3 HAPD

HAPD (Hybrid Avalanche Photo Detector) is a hybrid photon detector in which the dynode structure of PMT is replaced by APD. A motivation of the HAPD development is to reduce the cost of big PMTs by eliminating the complicated dynode structure which has more components and requires labor-intensive assembly work for mass production.

A 13" HAPD prototype is developed by Hamamatsu and the University of Tokyo group [2]. A photon hitting HAPD is converted to a photo-electron at the photo-cathode, the photo-electron is accelerated by a high electronic field up to 10$\sim$20 keV and bombed into the APD. Since the APD has a gain of $\sim$100, the HAPD achieves a high gain of $O(10^5)$. The HAPD has also several good features; a good timing resolution, a good single-photon energy resolution and a good collection efficiency of photo-electrons. The performance of the HAPD is shown in Table 2 with a comparison to some PMTs.

Although the 13" HAPD prototype is successfully developed, they have some difficulties to make a commercial product. One of the issues is the usage of very high electric field (10 $\sim$20 kV) between the photo-cathode and APD, which could cause a discharge sometimes. Hamamatsu will soon commercially produce the 8" HAPD which applies a lower voltage. For HAPDs, the high QE photo-cathode could be adopted.

2.4 Gas photomultiplier

A gas photomultiplier is a new type of photon-detector that could be applicable for the future neutrino experiments with a gigantic detector. The idea of the gas photomultiplier itself is not new, but there is

Table 2: Performance comparison of the 13" HAPD with some standard PMT's

Performance	13" HAPD	13" PMT (R8055)	20" PMT (for Super-K)
Single Photon Timing Resolution	190 ps	1400 ps	2300 ps
Single Photon Energy Resolution	24 %	70 %	150 %
Quantum Efficiency	20 %	20 %	20 %
Photo-electron Collection Efficiency	97 %	70 %	70 %
Power Consumption	<<700 mW	$O(100)$ mW	700 mW
Gain	10^5	10^7	10^7

a new idea to adopt MPGD (Micro Pattern Gas Detector) for electron multiplication. The MPGD is an established technology used in many applications. Recently, the large area MPGD up to 30×30 cm^2 is developed. The features of the gas photomultiplier with the large area MPGD are (1) large photo-coverage, (2) good position resolution on the photo-cathode, (3) potentially low cost, (4) small volume, and (5) potentially low background. For this development, the prototype gas photomultiplier with MPGD is developed [3]. The prototype adopts the UV sensitive CsI photo-cathode and demonstrates the single photo-electron sensitivity and the high resolution imaging. Although there are still many R&D items for the gas photomultiplier, it is interesting to keep watching the future progress.

2.5 LAPD

Another interesting idea about a new type of photon-detector is a Large-Area Fast Photo-detector, named "LAPD" under developments by the LAPD collaboration [4]. They have a three-years R&D program to make the commercializable modules. The features of the LAPD are (1) small cell size less than 300 μm for the good spacial resolution, (2) homogeneity to make uniform large-area, (3) very fast rise time and (4) intrinsically low cost. For the fine cell structure, a large-area Micro-Channel Plate Panel is considered. Before the LAPD is realized, there are many R&D subjects which the LAPD collaboration is currently addressing.

3 Photon-detectors for Fine-Grained Detectors

A high precision neutrino experiment requires a fine resolution tracking-type massive detector to identify the neutrino flavor unambiguously, to measure the neutrino flux accurately, and to study the type of neutrino interactions. For this purpose, several fine-segmented scintillator tracking-type detectors are developed with the fine multi-pixel photon-detectors: the K2K/SciBooNE SciBar detector [5, 6], the MINERνA detector [7], the T2K ND280 detector [8], and the NOνA detectors [9]. With the fine multi-pixel photon-detectors, the light from the fine-segmented scintillators through the wave-length shifting fiber are measured. The SciBar and MINERνA detectors used the multi-anode PMTs, the T2K ND280 adopts Hamamastu MPPC (Multi-Pixel Photon Counter) which is a kind of PPD (Pixelized Photon Detector), and the NOνA detector will use the multi-pixel APDs. We review the technology of the fine multi-pixel photon-detectors. In the next generation super-neutrino beam experiments, the high resolution neutrino detector will be designed by further improving those technologies. For a detector at the neutrino factory, the similar type of scintillator detector with larger size is also considered.

3.1 Multi-Anode PMT

A multi-anode PMT is a standard and matured device. The K2K SciBar detector uses Hamamatsu H8804 which has 8×8 anodes in one PMT. The anode size is 2×2 mm^2, and the uniformity over 64 anodes is 20 % in RMS. The response of each channel is linear up to 200 photo-electrons at the gain of 6×10^5. The similar multi-anode PMTs are used in the MINOS, OPERA and MINERνA experiments. The device is

compact and reliable. A few disadvantages of this device are non-applicable under the magnetic field, and the cost per anode is moderate (∼$30/anode).

An evolution of multi-anode PMTs is Hamamatsu Flat Panel PMT H9500. The H9500 model has a wider photo-coverage (52×52 mm^2) with more anodes of 16×16 in one package. It has a small dead space between anodes and achieves the fast response time although it is not tolerant to the magnetic field.

For an application of PMTs in the magnetic field, the MCP-PMT (Multi-Channel-Plate PMT) is developed. Tho multi-anode MCP-PMT is developed as a candidate photon-detector of the RICH (Ring-Image-CHerenkov) detector in collider experiments. Burle/Photonis provides the multi-anode MCP-PMT 85011-501 model. The 85011-501 has 8×8 anodes in 51×51 mm^2 area. It adopts MCP with 25(10) μm pore. A few disadvantages of these multi-anode MCP-PMTs are relatively low gain ($\sim 1 \times 10^5$) and high cost (∼$4000/PMT). Hamamatsu is also developing the multi-anode MCP-PMT, SL10 model. Hamamatsu SL10 is developed and tested for the KEK B-factory upgrade.

3.2 Multi-pixel APD

The FNAL NOνA neutrino experiment adopts the Hamamatsu S8550 Si Avalanche Photo-diode (APD)[1]. They develop the custom designed 32 channel APD with a low cost ($14/channel). An advantage of APD is very high QE which is 85% for the wavelength of 525 nm. Since the APD has only a gain of 100, it is operated at -15 degree to reduce the noise. They are successful to reduce the noise pulse hight less than 3 photo-electrons. Since they detect 30-39 photon-electrons for the minimum ionizing particles passing the far side of the detector, they reach the signal to noise pulse hight ratio to be $10:1$.

3.3 PPD

One of the most remarkable progress in the developments of the new photon-detectors happens to realize PPD (Pixelized Photon Detector) which was formerly called "SiPM (Silicon Photo-Multiplier)". The PPD consists of large arrays ($O(10^3)$) of tiny APD pixels which are operated in a limited Geiger mode. The outputs of PPD is the sum of the binary signals of hit APD pixels which corresponds to the count of photons. All over the world, there are many kinds of PPDs under development: SiPM (Silicon Photo-Multiplier), MRS-APD (Metal Resistive Semiconductor APD), SPM (Silicon Photo-Multiplier), MPGM APD (Multi-Pixel Geiger-mode APD), AMPD (Avalanche Micro-pixel Photo-Diode), SSPM (Solid State Photo-Multiplier), GM-APD (Geiger-Mode APD), SPAD (Single Photon Avalanche Diode) and MPPC (Multi-Pixel Photon Counter). Now the PPD is commercially available, and Hamamatsu produces and supplies MPPC (Multi-Pixel-Photon-Counter) to a market. In the commercial list of Hamamatsu, three types of MPPCs are available: one is a 100 pixel model with 100×100 μm^2 size of the pixel, the second is a 400 pixel model with 50×50 μm^2 pixel size, and the third is a 1600 pixel model with 25×25 μm^2 pixel size. All MPPC have 1×1 mm^2 active area.

The T2K ND280 detector adopts 60,000 specially customized MPPCs for the fine-grained detector, the electro-magnetic calorimeter, the Fe/Scinti sandwich neutrino beam monitor, the muon range detector and the π^0 detector. The specification of the T2K MPPC is summarized in Table 3. The cost of T2K MPPC is rough $20/device with the order of 60,000. T2K is the first experiment to use the large amount of PPD (and MPPC). So, the experience of T2K with MPPCs could be valuable to use PPD in the future neutrino experiments.

3.4 Multichannel HAPD

In Section 2.3, we introduced the large size HAPD. Here, we review the smaller size multi-channel HAPD. Since HAPD uses APD for electron multiplication and signal output, we can use a multi-pixel APD to make the position sensitive multi-pixel photon-detector. Hamamatsu develops the multichannel

[1]The detector technology of NOνA can be found in the other presentation in the workshop.

Table 3: Specification of T2K MPPC

Item	Specification
Active Area	1.3×1.3 mm^2
Pixel size	50×50 μm^2
Number of pixels	667
Operation voltage	70 V (typical)
Photon detection efficiency	$\sim$30 %
Dark Count (@gain=7.5×10^5)	< 1.35 Mcps (0.5 pe threshold)
	< 0.14 Mcps (1.5 pe threshold)

(144 channels) HAPD [10], primarily for the RICH detector in the KEK B-factory upgrade. Hamamatsu multichannel HAPD adopts four 36-pixel APDs in a photo-tube. An advantage of the multichannel HAPD is the operation in the magnetic field. The multichannel HAPD has an effective area of 64×64 mm^2 (65% active) with 4.9×4.9 mm^2 position segment. They achieve 25% QE, and the dark noise is 1500e with the operation voltage of APD at 300 V. The multichannel HAPD requires 8 kV between the photo-cathode and APD to accelerate the photo-electrons. The future progress of the device is interesting for an application in the neutrino detector.

4 Summary and Remarks

As we review the recent progress of photon-detectors in this paper, many types of photon-detectors with several key technologies exist and are under development. Necessary R&D, cost reduction, and commercial availability depend on the time scale when we need the photon-detectors and how many we use for neutrino detectors. For a gigantic Water Cherenkov/Liquid Scintillator detectors, the developments of large area photon-detectors with low cost (hopefully \$1k/device) is essential. We need further developments to realize the moderate-cost experiments. For fine-grained detectors with or without the magnetic field, the semiconductor photon-detectors have a great potential to become low cost. As an example, the cost of MPPC is around \$10$\sim$20/device, and the desired target might be $<$ \$10/device[2].

In addition to the developments of photon-detectors themselves, the developments of the electronics matching with photon-detectors are equally important. For this purpose, the design and production of ASIC and the custom electronics are also very active. They are developed to handle many thousands of channels, to be senstive to a low-gain small signal, or to record the fast response, etc.. The progress of the electronics with photon-detectors are promising and should be reviewed in near future.

Finally, the new type of photon-detectors could open the new applications (medical imagining, etc..) and new commercial markets. So, the development of photon-detectors could stimulate an technology innovation and contribute to the evolutio of science.

Acknowledgments

The work was supported by MEXT (Japan) and JSPS (Japan) with the Grant-in-Aid for Young Scientists S 20674004, Scientific Research on Priority Areas “New Developments of Flavor Physics”, the global COE program “The Next Generation of Physics, Spun from Universality and Emergence”.

References

[1] K. Nakamura, Front. Phys. **35**, 359 (2000).

[2] Y. Kawai *et al*., Nucl. Instrum. Meth. A **579**, 42 (2007).

[2]The Japan ILC group asks Hamamatsu to make MPPC with O(\$1)/device, although we have no answer yet.

[3] H. Sekiya, arXiv:0809.3319 [astro-ph].
[4] http://psec.uchicago.edu/other/Project_description_nobudgets.pdf
[5] K. Nitta *et al*., Nucl. Instrum. Meth. A **535** (2004) 147 [arXiv:hep-ex/0406023].
[6] K. Hiraide *et al*. [SciBooNE Collaboration] Phys. Rev. D **78**, 112004 (2008).
[7] K. S. McFarland [MINERvA Collaboration], Nucl. Phys. Proc. Suppl. **159**, 107 (2006) [arXiv:physics/0605088].
[8] M. Yokoyama *et al*., Nucl. Instrum. Meth. A **610**, 362 (2009) [arXiv:0807.3147 [physics.ins-det]].
[9] D. S. Ayres *et al*. [NOvA Collaboration], arXiv:hep-ex/0503053.
[10] S. Nishida *et al*., Nucl. Instrum. Meth. A **610**, 65 (2009).

Cost effective electronics for LAr and photo-detectors readout

Sandro Centro
University of Padua, Padova, Italy

Abstract
The T600 ICARUS detector has a DAQ system that has proved a quite satisfactory performance in the test run performed in Pavia in summer 2001.
The electronics has been described in various papers and technical notes. In this paper, starting from the experience gained in the T600 operation, we propose an upgraded DAQ scheme that implements the same basic architecture with more performing new components and different modularity in view a multi-kton TPC (e.g. MODULAr) with a number of channels in the order of ~$n*10^5$.
Also the electronics for PMTs detecting scintillation light in Ar will be shortly presented.

1 T600 DAQ

The ICARUS T600 read-out architecture was designed for a detector with few 10^4 channels.
The analog chain consists of a front-end low noise charge sensitive pre-amplifier, based on a custom designed BiCMOS dual channel IC with j-Fet input stage, followed by a baseline restorer to reduce low frequency noise. The gain of the front-end amplifier and filter is $1V/164fC$. The $10bit$ ADC input range is $1V$, and then the least count is equivalent to 1000 electrons. This value matches with the amplifier noise of ~1250 electrons with a detector capacitance of $450pF$ (signal wires plus cables).

The basic modularity of the system is 32. The digitizing stage consists in a set of 32 channels connected to four 8-to-1 multiplexer, each one followed by a $10bit$ ADC sampling at $20MHz$. The sampling time is then $400ns$ per channel.

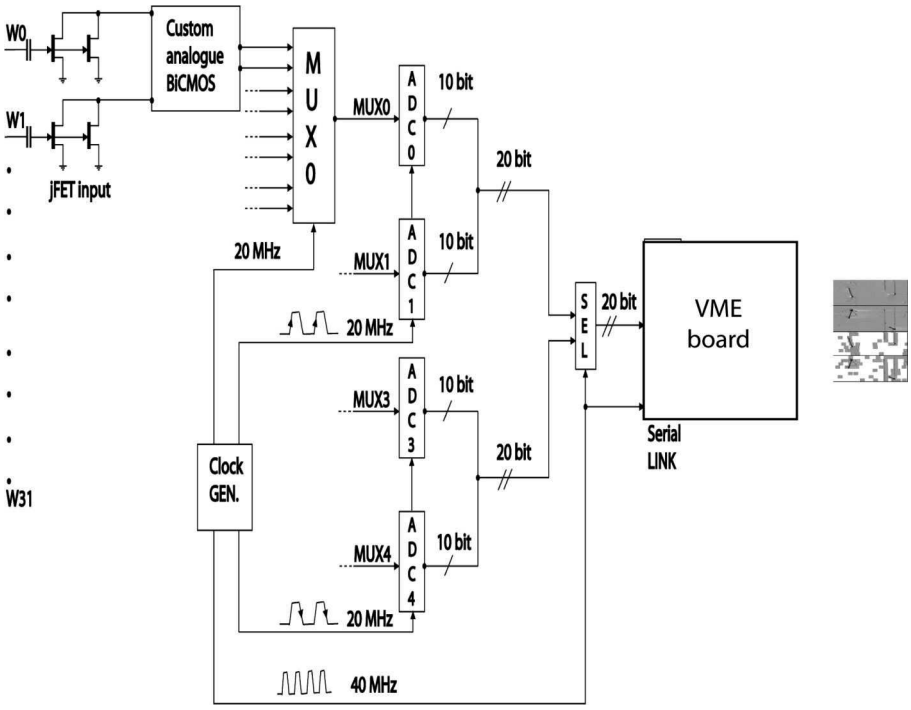

Fig. 1: Diagram of ICARUS DAQ

For each group of two ADCs the two 10*bit* outputs are merged in a 20*bit* word. As the positive clock edge drives one group of two ADCs and the negative clock edge drives the other group of two, 20*bit* words can be transmitted at 40*Mhz* rate on single 20 *bit* wide channel. This scheme is implemented on a single VME-like analog board (CAEN V789) hosting the 32 channels amplifiers, ADCs together with a 20*bit*,

40*MHz*, serial link that allows sending the data to a second digital board (CAEN V791) that performs buffering of events. The serial link is LVDS (Low Voltage Differential Signaling) and serializes the 20*bit* data and clock on four copper lines with an equivalent data throughput of 800*Mbps*. The block diagram is in Fig. 1.

The receiving digital board, named ARIANNA, hosts two custom-made feature extraction ASIC chips (DAEDALUS) for hit finding, zero skipping and self-triggering. Each of the two DAEDALUS chips operates on the data stream of a set of 16 channels and controls also the circular memory buffer. DAEDALUS includes also a median filter to reduce high frequency noise. A 28*bit* absolute time register is associated to each data buffer in the memory to allow alignment of data in the event reconstruction. The board complies with the VME electrical and mechanical standard.

This architecture has proven to be well suited for the T600 detector and to perform accordingly the expectations.

2 Critical issues

It is important to remember that the DAQ architecture for T600 was conceived in 1997 and DAEDALUS and front-end dual channel BiCMOS circuits were designed in 1998. The full system (~50,000 channels) was designed and built from 1999 to 2000.

Even if the architecture proved to be very performing, nowadays it would not be possible to replicate the same circuits, as they are, because many basic components are now discontinued.

In this scenario it is very important then to make a critical analysis of the whole system to spot the areas where the necessary changes could led to a more efficient structure.

Adopting a top down approach one evident limitation of the T600 DAQ is due to the adoption, perfectly legitimate at that time, of the VME standard for the digital boards. For the analog boards the same 6U Eurocard standard was adopted, with a custom backplane to connect the inputs from wires and distribute common signals (ADC baseline bias, enable signals, test pulses, etc.).

In the T600 DAQ 18 ARIANNA digital boards are housed in one VME crate that serves a total of 576 channels. One crate is connected to an analog crate, with the same modularity, which in turn receives the signals from a single T600 flange that in fact has 18 feed-through connectors, one for each set of 32 channels. Configuration and control of the 18 boards relies on a dedicated VME cpu, which also handles the data transfers from board buffers to the Ethernet event builder network. Performance of the DAQ system is bounded by the VME (8-10 MB/s), together with the sequential order single board access mode inherent to the shared bus architecture.

The redesign of the system can overcome this limitation adopting a modern switched I/O, as PCI Express standard for instance, allowing the parallelization of the data flows. In addition such I/O transaction can be carried over low cost optical gigabit/s serial links. This allows a more effective modularity of the digital hardware architecture, decoupled from the geographical distribution of the signal feed-through, thus lending to a larger integration and the consequent lower cost per channel.

3 The amplifier

Considering now the analog front-end does it not seem that a completely new design could improve either the *S/N* or the density (channels per package).

In a multi-kton TPC we can foresee wires with a pitch larger than the 3*mm* used in the T600. The adoption of 6*mm* pitch for MODULAr seems reasonable and will permit to use most of the existing molds and tools for wires support.

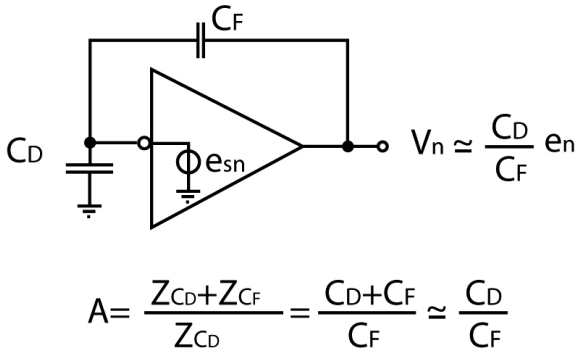

Fig. 2: Input amplifier equivalent circuit

The capacitance associated to each channel will be determined by the capacitance of the wires, in the order of 20*pf/m*, in parallel with the capacitance of the cable, in the order 50p*F/m*. Let's assume in the following discussion ~600*pF* as a reasonable value for 10*m* electrode wires, 6*mm* pitch, and average 8*m* of cable.

The dominant noise in a high capacitance detector, [5] [6] [7] [8], is the series noise e_{sn} (voltage noise) linearly increasing with the input total capacitance (C_D) while the parallel noise (current noise) contribution is proportional to the shaping time of the signal.

The equivalent circuit showing the effect of the input capacitance on the serial noise is given in Fig.2.

The serial noise generator has a noise density

$$e_{sn}^2 \propto \frac{T}{g_m} \tag{1}$$

where g_m is the transconductance of the input device. At the amplifier output the noise N becomes

$$N = e_{sn}\frac{C_D}{C_F} = \sqrt{\frac{T}{g_m}}\frac{C_D}{C_F} \tag{2}$$

In fact what really matters is the ratio signal to noise (S/N) that, considering the signal S proportional to $1/C_F$, being C_F the integrating capacitance, is

$$S/N \propto \frac{1}{C_D}\sqrt{\frac{g_m}{T}} \tag{3}$$

We need the use of high transconductance front-end components or lower the working temperature of the amplifier. This latter issue will be discussed later.

The best component would be the bipolar transistor that typically exhibits transconductances in the order of

$$g_m \approx 400mS @ I_C = 10mA \tag{4}$$

with an amplification *merit factor* ($g_m * Z_{out}$) higher than $3\text{-}4*10^5$.

Second in the list would be j-Fet transistor that however has much lower transconductance, in the order of

$$g_m \approx 40mS @ I_C = 10mA \tag{5}$$

with a *merit factor* around 3-4$*10^3$.

However the bipolar transistor has a typical parallel noise density i_p= 1-2$pA/Hz^{.5}$ that with signals with a time extension of the order of 6-10μs, like in a liquid Argon TPC working at 500-1000V/cm, gives an unsustainable noise contribution.

The j-Fet then, with its quite reasonable transconductance and negligible parallel noise (i_p=.001 $pA/Hz^{.5}$, three order of magnitude lower), is an obliged choice. In terms of serial noise density the typical figure for a suitable component is ~1-2 $nV/Hz^{.5}$.

Normally we don't even consider CMOS for the extremely low transconductance and unfavorable *merit factor*. However recently, for space application, CMOS have been used for low temperature design. In this workshop an interesting poster on a front-end amplifier for use in liquid Ar has been presented [n]. The issue of mounting electronics inside the dewar will be presented later.

In liquid Argon a m.i.p. releases ~4000 electrons per mm, that means 2 *fC/wire* in case of 3*mm* or about twice for 6*mm* pitch. The Icarus amplifier, designed with dual j-Fet input, has an ENC of ~1250 electrons at C_D=450pF.

In Fig.3 an image from a LAr TPC is shown as an example. In Fig.4 signals along adjacent wires, belonging to the short track in the black box, are given. The overall gain at the ADC output is

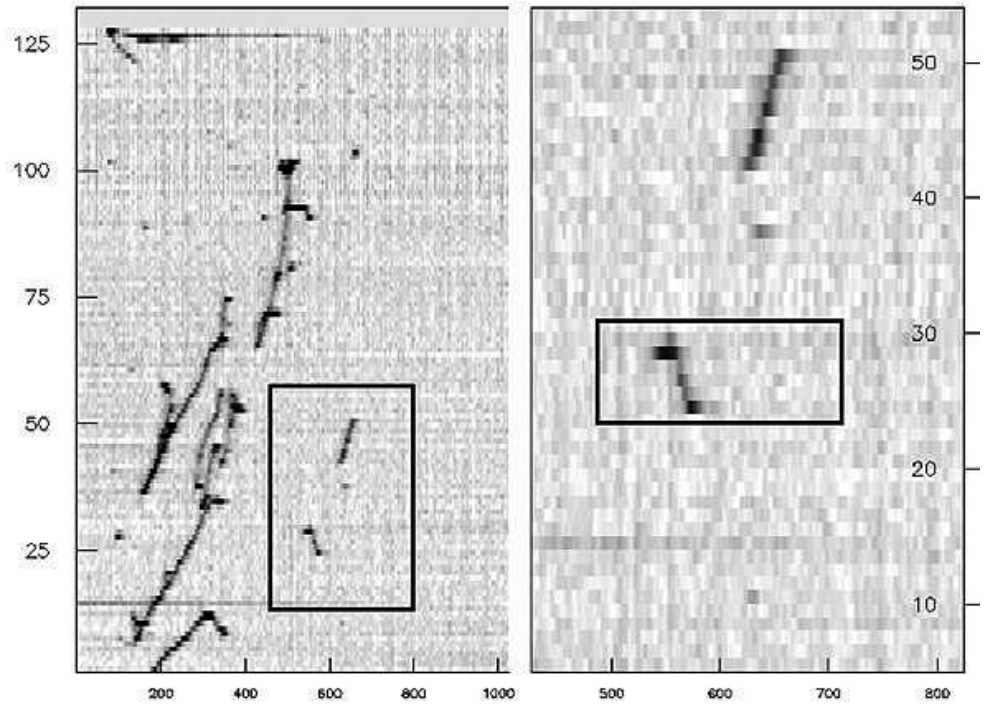

Fig. 3: At left: image of a low energy electromagnetic shower in a LAr TPC. Drift time is along X-axis (400ns sampling). Wire numbering is on the Y-axis (2.54mm pitch). At right: zoom of the selected area in the black box on the left image. The waveforms of the wires selected in the box at right are plotted in Fig.7.

~6 *counts/fC*, being the r.m.s. noise 1.2 counts (~1250 electrons at C_D=450pF) we reach a *S/N*=~10. With a pitch of 6*mm* we could keep the same *S/N*.

The custom IC [8] designed for the T600 front-end electronics in BiCMOS technology, has the typical structure of an unfolded cascode integrator, allowing however the connection of external j-Fet

at the input. In principle it would have been possible to include the j-Fet inside the monolithic device but unfortunately in BiCMOS technology j-Fet are obtained as a byproduct and their characteristics are totally unsatisfactory in term of gain and noise not to mention the fact that the silicon surface needed for a j-Fet with the required transconductance would be of the order of ~0.5mm^2.

In the T600 electronics we connected two discrete j-Fet in parallel to reach a total g_m of the order of 50-60mS. This solution seems suitable also for large TPC with C_D less than ~1000pF.

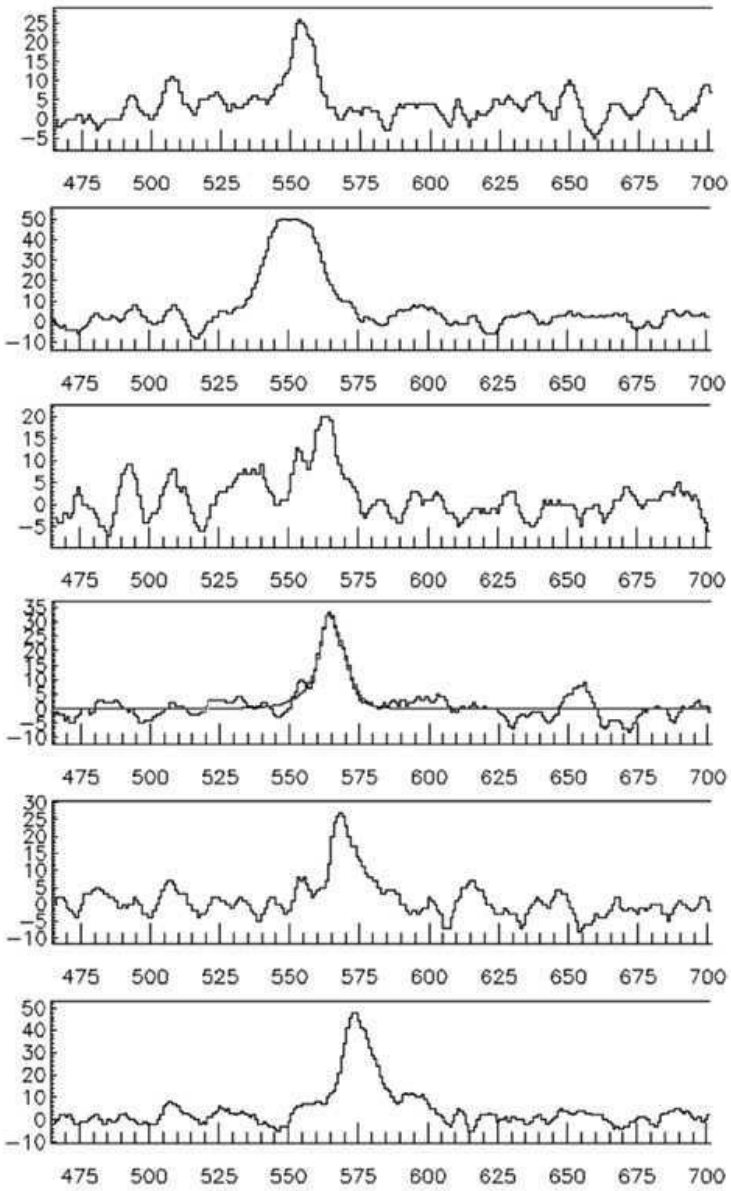

Fig. 4: Waveforms of the wires in the right box selection of Fig. 3, showing the typical signal shapes of minimum ionizing particles.

3 Cold electronics

In some proposals [mm] cold electronics mounted inside the detector is presented. In many cases it concerns only the amplifier, but in some case also the AD converters and digital processors are thought mounted inside.

According to (3) advantages of cold electronics are the reduction of the input capacitance because of shorter cables, the increase of the j-Fet transconductace g_m, and the reduction of the temperature *T*. In Figure N the typical transconductace curve as a function of the temperature is given. The improvement of the *S/N* will be a factor 2.4 due the combined effect of lower Johnson noise [~1.9] and 60% higher transconductance [~1.26].

However the effect of shorter cables will be limited as it is not conceivable to mount each amplifier at the end of the corresponding wire. Even inside the detector the amplifiers will be grouped on cards, so the only part of connection saved is the one from the detector feed-through to the external electronics crates. A proper design of electronics crate for external electronics would eliminate external cables.

A real disadvantage of cold electronics is the limited design architectures due the limited choice of active components working at 86ºK, largely compensating the improvement of *S/N*.

But the reason why the cold electronics will not pay is another. A multi-kton TPC will require tens of years for R&D and construction and eventually will run for other tens of years. It is not conceivable to prevent any possible upgrade of the only part of the detector that could be modified and could benefit of the technological evolution of electronics in the future decades.

A new front-end layout for a future large detector can be hosted in a compact crate very close to the feed-through flange. Or even one could think to use the flange itself as a backplane supporting the analog boards. This solution is under study and a possible layout will be shown. The number of connectors and cables would be drastically reduced with a benefit for cost and *S/N*.

The new modularity will be the number of channels served by one feed-through flange. In the solution under development we use the modularity of the Icarus flange that serves 576 channels.

This new 576 channels module under study must also perform the data conversion before transmitting data to the digital buffering board as will be described.

4 AD Conversion

A list of suitable ADC is given in Table I. All of them are serial ADCs that provide the converted data as a sequence of *bit*s high rate. The Freq. given in the table refers to the sampling frequency. The date rate of the serial *bit*s is typically around 10-12 times higher. For instance to reach the 3*MHz* sampling rate, AD7273 must be clocked at 48*MHz*.

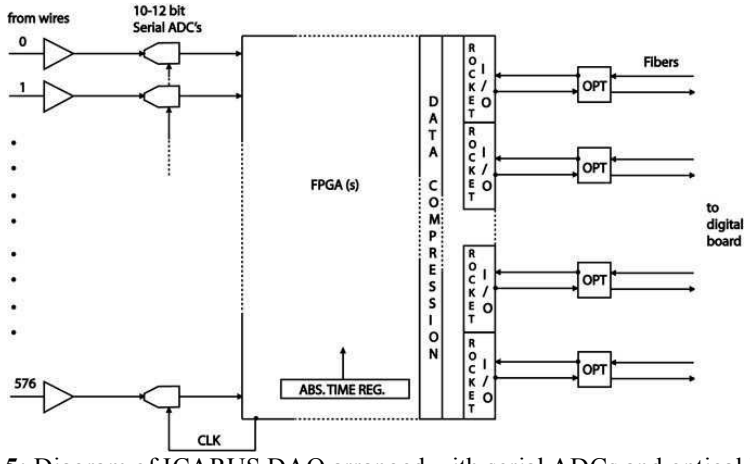

Fig. 5: Diagram of ICARUS DAQ arranged with serial ADCs and optical link.

These devices are quite interesting for price, power consumption and dimensions. Typically they are packed in Mini Small Outline Package (MSOP) smaller than $5x5\ mm^2$.
The choice is rather large and we can expect that more products will be available within one year.

The acceptable sampling frequency for a TPC with 6 *mm* pitch can be assumed in the range of 1-1.5*Mhz* for which there is already a wide choice of devices.

We can assume a resolution of 10*bit* but also 12*bit* ADCs are available. The arrangement of the ADCs after the amplification is given in Fig. 5.

Assuming a sampling frequency of 1.5*Mhz*, and 10*bit* ADCs, and data compression in one byte, we need to transmit 6912*Mbit/s*, that on an optical fiber, to balance zeros and ones becomes 8640*Mbit/s*. Optical links with 1.5*Gbit/s* data rates are standards and can be driven by the RocketIO™ interfaces available on many FPGA from different vendors. Six optical links could serve all the channels of one module (576) and convey also extra information as absolute time. Some of the links will be bidirectional to distribute absolute clock and simple commands.

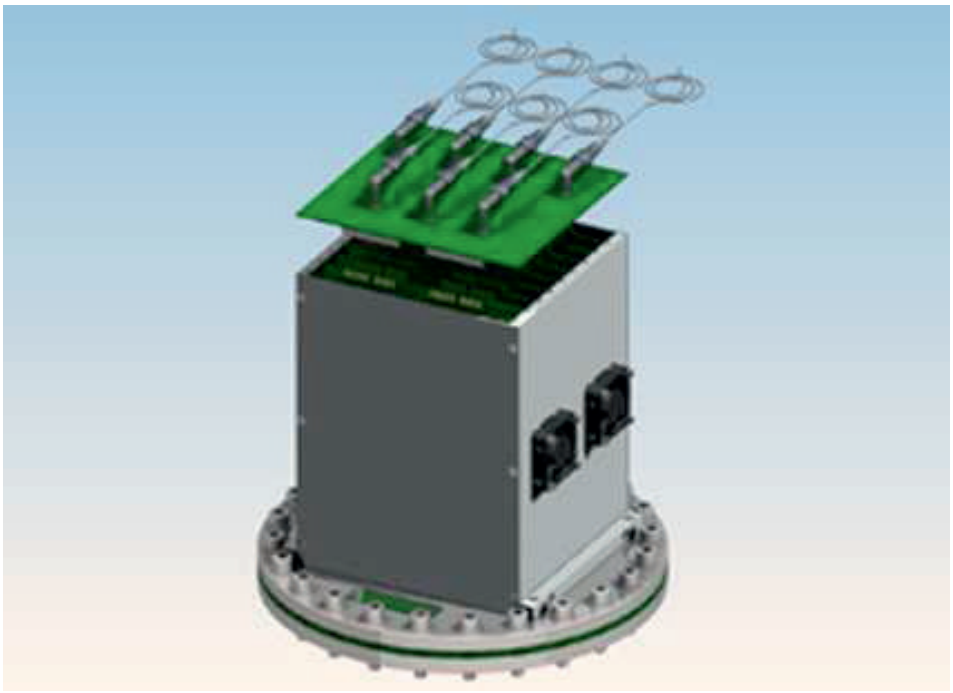

Fig. 6: Artistic view of ICARUS DAQ mounted on the flange with serial ADCs and optical link.

The ADCs and FPGAs will be housed in the same crate next to the flange or even on special boards on top of the amplifiers boards shown in Fig.6.

What will not be discussed in this paper is the implementation of the equivalent of the ARIANNA board. One could say that nowadays for hit finding ASIC VLSI will not be required as the feature extraction algorithm can be implemented in powerful FPGA.

5 Photo-detectors readout

Ionization in liquid Argon (LAr)is accompanied by scintillation light emission. The two processes are complementary and their relative weight depends on the strength of the electric field (recombination) and *dE/dx*.

Electron yield, Y_{ion}=~2.9*10^4 e^-/MeV, and photon yield, Y_{ph}=~2.4*10^4 γ/MeV, are similar for a m.i.p. at an electric field of 500*V/cm*.

Light is emitted at 128*nm*, its detection generally requires wave-length shifters, with two components exponential decay: one short time constant, $\tau_s \sim 6ns$, and one long time constant, $\tau_L \sim 1.5\mu s$.

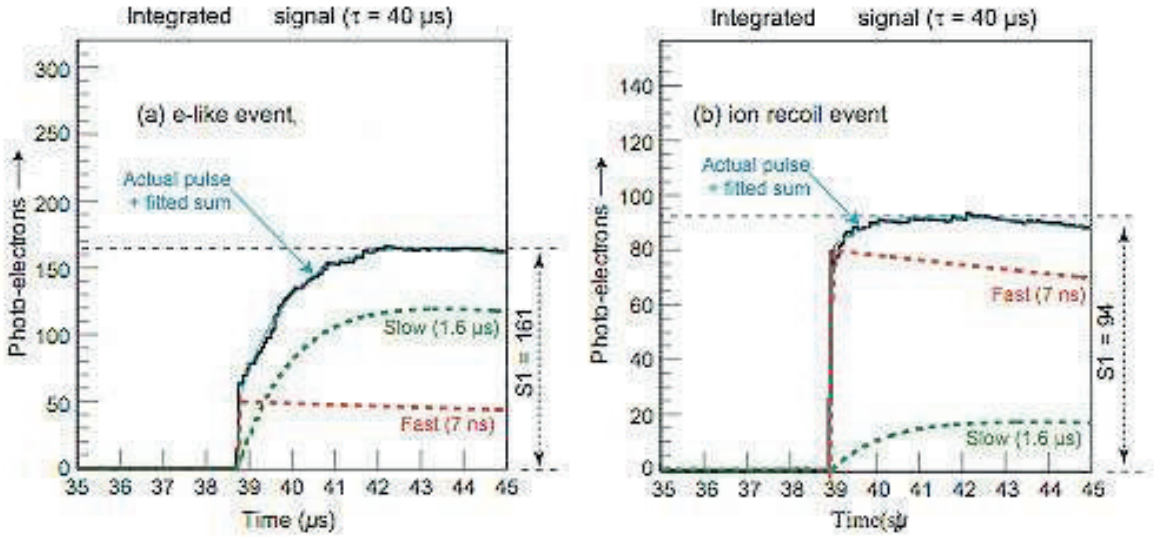

Fig. 7: Integrated signals for electron like events and ion recoils.

Prompt light signal is typically used for trigger (e.g. Icarus) or for particle identification (e.g. WArP). In fact for a m.i.p. about 25% of emitted light has short time constant and about 75% has long time constant, while a recoil has about 75% of the emitted light with short time constant and about 25% with long time constant. In Fig. 7 integrated signals for electron like events and ion recoils are given.

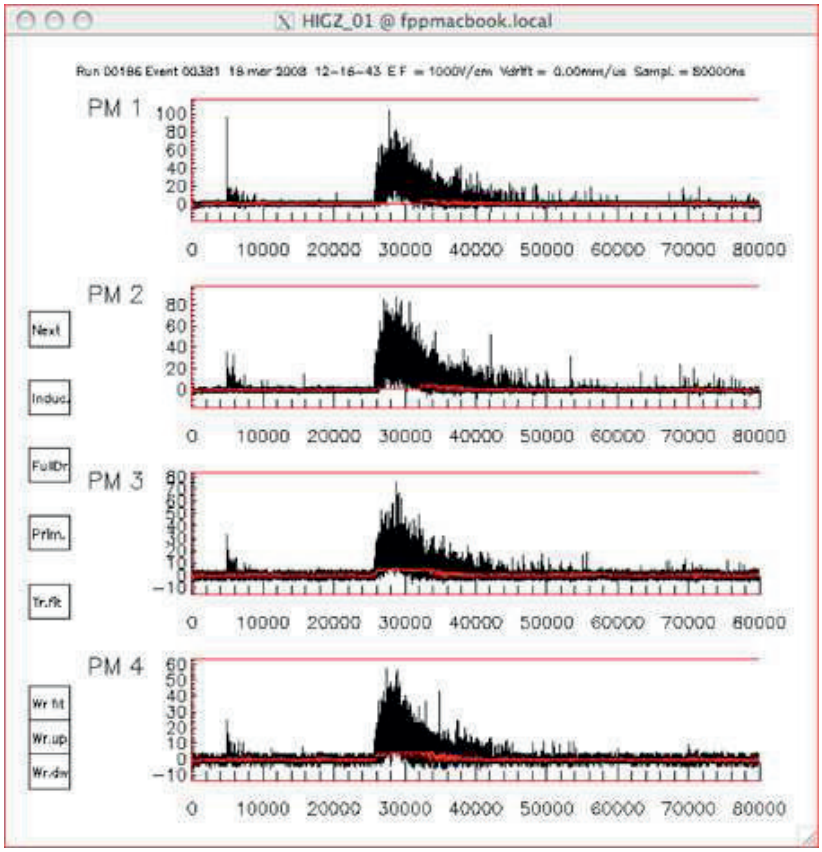

Fig. 8: At left S1 and at right S2 signals from WaRP.

In double phase (liquid and gaseous Argon) detectors, one can distinguish the primary scintillation, S1, in liquid, from the scintillation in gas, S2, proportional to extracted ionization

electrons. S1 and S2 have similar characteristics and can be studied in detail identifying individual electrons through high frequency, high priced, waveform recorders with sampling frequency in the gigahertz range. In Fig. 8 typical S1 signals (left) and S2 signals (right) from WArP detector are shown.

We can expect in the future the appearance on the market of competitive products at reduced price.

The layout foreseen for charge signals that uses the flange as electronics backplane can be exploited also in case of photons signals.

Bibliography.

[1] Carpanese C. et al., ARIANNA: the ICARUS Experiment Readout Module. IEEE Trans. on Nucl. Science. vol. Vol. 45 no. 4 (1998), pp. 1804-1808 ISSN: 0018-9499.

[2] Carpanese C. et al., DAEDALUS: a hardware signal analyser for ICARUS. Nucl. Instr. and Meth A (1998) 409, pp. 294 ISSN: 0168-9002.

[3] Centro S. et al., Performance Evaluation of a Hit Finding Algorithm for the ICARUS Detector. Nucl. Instr. and Meth A (1998) 412, 2-3, pp. 440 ISSN: 0168-9002.

[4] Amerio S. et al., Design, construction and tests of the ICARUS T600 detector, Nucl. Instr. and Meth A (2004) 527, 329-410.

[5] V.Radeka, Design of a Charge Sensitive Preamplifier on High Resistivity Silicon. IEEE Nuclear Science Symposium , 35, no. 1, Feb. 1988.

[6] Centro S., Signal amplification for high capacitance ionization chambers, Nucl. Instr. and Meth A (1992) 315, 404-410.

[7] Bacci C. et al., A Hybrid Charge Sensitive Amplifier for High Capacitance Detectors, Nucl. Instr. and Meth A (1988) 273, 321-325.

[8] Centro S. et al., Low-Noise BiCMOS Front-End and Fast Analogue Multiplexer for Ionization Chamber, Nucl. Instr. and Meth A (1998) 409, pp. 300 ISSN: 0168-9002.

[9] Lengeler B., Cryogenics, Semiconductor Devices Suitable for Use, Cryogenic Environments, vol. 14, no. 8 (1974), pp. 439-447.

[10] Kirschmann R. K., Cold Electronics: an Overview. Cryogenics Environments, vol. 25, no. 3 (1985), pp. 115-122.

[11] S.Rescia and D.Stephani Reliability of Preamplifiers at Cryogenic Temperatures. BNL, GEM TN 93-339.

[12] P.Cennini et al., A 3-D Image Chamber for the Liquid Argon TPC based on Multi-layer Printed - Circuit Board. NIM-A 346 (1994) 550-556.

[13] F.Lobkowicz and G.DiLoreto, Boiling near Preamplifiers in LAr Calorimeters. University of Rochester NY 1 July 1991.

[13] F. Goodenough, N-Channel JFET Process Makes Possible Low-Cost Low-Noise Charge-Amplifiers ICs, Electronics Design, January 22, 1996.

Kinematical analysis with the Emulsion Cloud Chamber in the OPERA experiment

F. Di Capua on behalf of the OPERA Collaboration
INFN, Napoli, Italy

Abstract

The OPERA experiment aims at measuring for the first time neutrino oscillation in appearance mode through the detection of ν_τ in an almost pure ν_μ beam produced at CERN SPS (CNGS), 730 km far from the detector. The ν_τ appearance signal is identified through the measurement of the decay daughter particles of the τ lepton produced in CC ν_τ interactions. Since the short-lived τ particle has, at the energy of the beam, an average decay length shorter than a 1 mm, a micrometric detection resolution is needed. The OPERA apparatus is hybrid, using nuclear emulsion as high precision tracker and electronic detectors for the time stamp, event localization in the target and muon reconstruction. The Emulsion Cloud Chamber technique fulfils the requirement of a microscopic resolution together with a large target mass. The kinematical analysis allowed by this technique is described.

1 The ECC in the OPERA experiment

The short-lived τ lepton ($c\tau$ = 87.11 μm) is identified by its characteristic decay topologies either in one prong (electron, muon or hadron) or in three-prongs; its short track is measured in a target made of 1 mm thick lead plates (target mass and absorber material) interspaced with nuclear emulsion films (high-accuracy tracking devices). The films are made of two 45 μm emulsion layers on each side of a plastic base of 200 μm. This detector is historically called Emulsion Cloud Chamber (ECC).

OPERA has a modular target with units (called bricks) consisting of 57 emulsion films [1] interleaved with 56 lead plates. The transverse dimensions are 12.8 $\times$ 10.2 cm^2 and the thickness along the beam z direction is 7.9 cm (about 10 radiation lengths). The weight is 8.3 kg. The OPERA experiment contains 150000 bricks in total.

The scanning of emulsion films is performed with two different types of automatic microscopes: the European Scanning System (ESS) [2, 3] and the Japanese S-UTS [4]. Microscope systems have comparable performances ensuring a scanning speed two orders of magnitude greater than that of the systems used in the recent. The spatial and angular resolution is of the order of $\sim$1 μm and 1 mrad, respectively.

In order to reduce the emulsion scanning load, interface films (Changeable Sheets, CS [5]), between the electronic detectors and the bricks are used. They consist of tightly-packed emulsion film doublets, glued on the downstream face of each brick. CS doublets are removable without opening the brick. All tracks measured in the CS are sought in the most downstream films of the brick and followed back until they disappear in three consecutive films. The stopping point is considered as the signature either for a primary or a secondary vertex. The existence of the vertex is then confirmed by scanning a volume of about 2 cm^3 around the stopping point.

2 Topological and kinematical analysis

The ECC allows a very precise position determination of the primary neutrino interaction vertex. The track impact parameter distribution of the reconstructed tracks with respect to the reconstructed vertex position is shown in Figure 1.

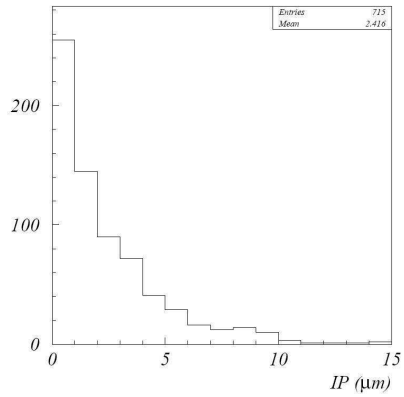

Fig. 1: Impact parameter distribution of the tracks in OPERA neutrino events with respect to the reconstructed vertices.

As expected, the impact parameter distribution is peaked at zero with a mean value of 2.4 μm. The few entries above 10 μm are identified to be due to low energy particle tracks.

A kinematical characterization of the neutrino interaction is also possible in ECC. The relevant aspects will be discussed in the following.

2.1 Momentum measurement

An estimation of charged particle momenta is possible by detecting the deviations of the particle trajectory from a straight line due to multiple coulomb scattering (MCS). In fact the distribution of track slope differences after crossing a fixed amount of lead plates is peaked at zero with a shape which can be approximated by a Gaussian with a standard deviation given by

$$\theta_0 = \frac{13.6\text{MeV}}{pc\beta}\sqrt{\frac{x}{X_0}}\left(1 + 0.038\ln(\frac{x}{X_0})\right). \quad (1)$$

The angular resolution of the emulsions allows the momentum measurement of charged particles ranging from hundreds MeV to a few GeV. It corresponds to the momentum range of the secondary hadrons produced in OPERA neutrino interactions. By using dedicated test beam with pion of known momentum, a momentum resolution from 20% to 40% for pion momentum from 1 GeV/c to 8 GeV/c has been achieved with this method.

2.2 Electron identification

The ECC allows an excellent electromagnetic shower identification, hence the separation of electrons and pions. An electron quickly develops an electromagnetic shower in lead. The total number of tracks, as well as the different longitudinal and transverse profile of the shower can be used for particle identification. On the other hand the MCS angle presents a different longitudinal profile for electrons and pions: going through a material the energy remains almost constant for pions while it exponentially decreases for electrons. By using a Neural Network method an electron identification efficiency of 90% with a π contamination less than 1% has been obtained at energies greater than 2 GeV. For $E = 1GeV$ the electron identification efficiency is 80% with a π contamination of 1% [6]. By counting the segments of the shower, as it is done in a calorimeter, a measurement of electron energy is possible.

The good shower reconstruction capability can be also used for π_0 identification. By reconstructing the two separate showers from $\pi_0 \rightarrow \gamma\gamma$ decay, the invariant mass of the π_0 can be measured with

a resolution of 30%. In Fig.2, the display of an OPERA neutrino interaction reconstructed in ECC is shown: six showers are reconstructed in the event, four of them are due to π_0's produced at primary vertex, the other two origin from a π_0 produced at secondary hadronic interaction.

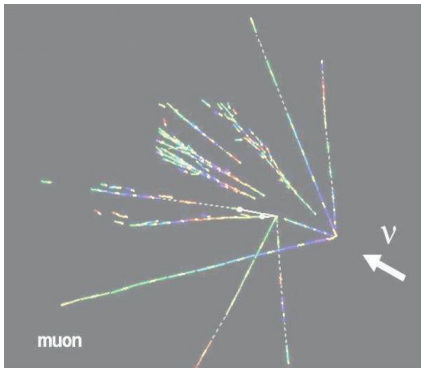

Fig. 2: A neutrino interaction reconstructed in ECC with a secondary hadron interaction. Six electromagnetic showers have been reconstructed in the event: four of them from the primary and two from a secondary vertex.

3 Charm events

Charmed hadrons produced in neutrino interactions decay with a flight path similar to the one of the τ lepton. The capability of the ECC in the detection of short-lived particles is demonstrated with the detection of first charm events in the OPERA experiment. Fig.3 shows the display of two neutrino interactions where a charmed hadron is produced. On the left side a D^0 decay in four charged particles is shown, the flight length of the D^0 is about 300 μm; the angle between the muon and D^0 direction in the transverse plane is 173°. On the righ a charged charm decay in single prong is shown, the flight length is about 3 mm, the angle between the muon and the charm direction in the transverse plane is 165°.

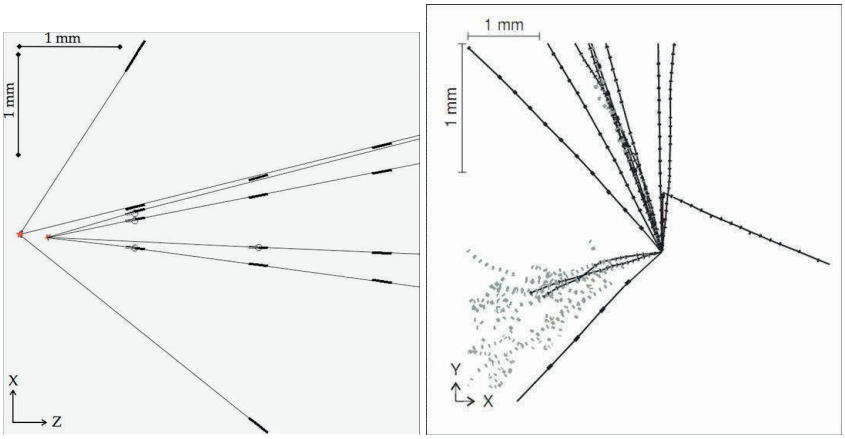

Fig. 3: Left: D^0 decay in four charged particles. Right: Charged charm decay in one prong.

References

[1] T. Nakamura *et al.*, Nucl. Instrum. Meth. A **556**,(2006) 80.

[2] G. Rosa *et al.*, Nucl. Instrum. Meth. A **394**, 357 (1997);
N. Armenise *et al.*, Nucl. Instrum. Meth. A **551**, 261 (2005);
M. De Serio *et al.*, Nucl. Instrum. Meth. A **554**, 247 (2005);
L. Arrabito *et al.*, Nucl. Instrum. Meth. A **568** 578 (2006);
I. Kreslo *et al.*, JINST **3** (2008) P04006.

[3] L. Arrabito *et al.*, JINST **2** P05004 (2007).

[4] S. Aoki *et al.*, Nucl. Instrum. Meth. B **51**, 466 (1990);
T. Nakano, PhD Thesis, University of Nagoya (1997);
T. Nakano [CHORUS Collaboration], *International Europhysics Conference on High-Energy Physics* (HEP 2001), Budapest, Hungary, 12-18 July 2001.

[5] A. Anokhina *et al.* [OPERA Collaboration], JINST **3** P07005 (2008). Nucl. Instrum. Meth. A **401**, 7 (1997).

[6] L. Arrabito *et al.*, JINST **2** P02001 (2007).

A search for $\nu_\mu \rightarrow \nu_\mathrm{e}$ oscillations in the MINOS experiment

J.J. Evans (for the MINOS collaboration)
Department of Physics and Astronomy, University College London, Gower Street, London, WC1E 6BT, United Kingdom

Abstract
The MINOS experiment uses the NuMI neutrino beam to make precision measurements of the neutrino mixing parameters. A beam of ν_μ is produced at Fermilab. Its energy spectrum is measured near the production point, and again after 735 km at the Soudan Underground Laboratory. By looking for ν_e appearance in the beam, limits can be placed on the as yet unmeasured mixing angle θ_{13}. At the far detector (in the Soudan laboratory), 35 ν_e candidate events are observed with a predicted background of $27\pm5(\mathrm{stat.})\pm2(\mathrm{syst.})$ events: a 1.5σ excess. At 90% C.L. this gives an upper limit range of $\sin^2(2\theta_{13}) < 0.28$–$0.34$ for the normal neutrino mass hierarchy and $\sin^2(2\theta_{13}) < 0.36$–$0.42$ for the inverted hierarchy, depending upon the CP-violating phase δ_CP.

1 The MINOS experiment

The MINOS experiment uses the NuMI ν_μ beam, produced from 120 GeV protons at the Fermilab accelerator complex in Chicago. The beam consists of 98.7% $\nu_\mu + \overline{\nu}_\mu$ and 1.3% $\nu_\mathrm{e} + \overline{\nu}_\mathrm{e}$. The neutrino energy spectra are measured at the near detector (ND), 1 km from the source, before oscillations have had time to occur. They are then measured again at the far detector (FD), 735 km from the source at the Soudan Underground Laboratory in northern Minnesota. Comparing the energy spectra at the two detectors allows the relevant oscillation parameters to be measured.

The two detectors are of similar design to reduce systematic uncertainties due to neutrino interaction physics, beam flux and detector response. They are tracking, sampling calorimeters consisting of alternate planes of 2.54 cm-thick steel and 1 cm-thick scintillator strips of 4 cm width [1].

If θ_{13} is non-zero a small fraction of ν_μ will oscillate to ν_e. If θ_{13} is at the Chooz limit [2], MINOS can detect this ν_e appearance to make the first measurement of a non-zero θ_{13}. At $\sin^2(2\theta_{13}) = 0.15$, 11 signal and 27 background events would be observed. The ν_e appearance probability for MINOS is

$$P(\nu_\mu \rightarrow \nu_\mathrm{e}) = \sin^2(2\theta_{13})\sin^2(\theta_{23})\sin^2\left(\frac{\Delta m^2_{\mathrm{atm}} L}{4E}\right) \qquad \text{(to leading order).}$$

2 Electron neutrino event selection

The MINOS detectors are optimized for the identification of charged current (CC) interactions of muon-type neutrinos and neutral current (NC) interactions of any neutrino flavour. They are therefore designed for muon tracking and hadronic shower calorimetry. The signal for this analysis is the CC interaction of electron neutrinos, producing an electromagnetic (e.m.) shower in the detector, characterized by a denser energy deposition near the event vertex than in a hadronic shower. The detector granularity is not optimal for distinguishing e.m. from hadronic showers: for e.m. showers, the radiation length in steel is 1.76 cm, compared to the 2.54 cm steel thickness; the Molière radius is 3.7 cm, compared to the 4.1 cm scintillator strip width. A typical 2 GeV ν_e-CC event covers 8 planes and 4 strips.

A number of preselection cuts are used to reduce the NC and ν_μ-CC backgrounds:

- The length of any track must be less than 25 planes.
- The number of track-only planes must be fewer than 16.

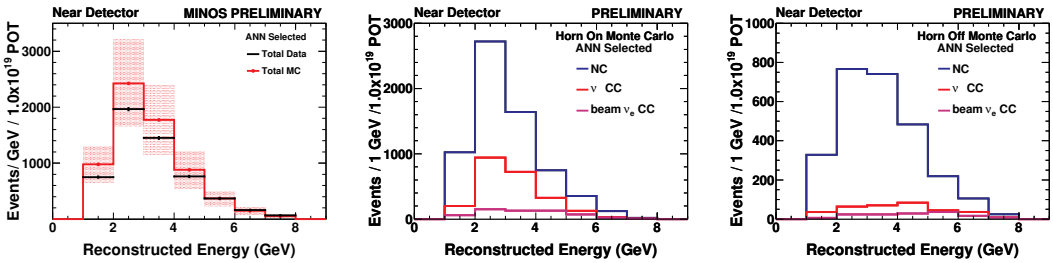

Fig. 1: Left: the reconstructed energy spectrum of ν_e-CC-like events at the near detector, comparing data (black) and simulation (red, with systematic error shown as the light red band). Centre: the composition of the sample with the NuMI beam focusing horns switched on; right: the composition with the focusing horns switched off.

– The reconstructed energy of the event must be between 1 GeV and 8 GeV.
– The event must contain at least one shower with more than four contiguous planes and greater than 0.5 MIP (minimum ionizing particle) of energy deposition.

This preselection takes the signal to background ratio to 1:12 from 1:55 (assuming $\sin^2(2\theta_{13}) = 0.15$).

A more sophisticated selection algorithm is required to further improve the sample purity. To do this, variables are formed which characterize the shower shape, length and width. Eleven such variables are combined into an artificial neural network (ANN) [3], shown in figure 2. This takes the signal:background ratio to 1:4 (for $\sin^2(2\theta_{13}) = 0.15$) with a signal efficiency of 41%, NC rejection power of 92.3% and ν_μ-CC rejection power of 99.4%.

3 Background correction

The ν_e-selected ND data and simulation disagree by up to 20%, as shown in figure 1. This is expected, since the selection cuts hard to reduce backgrounds, leaving only tails of distributions. The two-detector nature of MINOS means the ND data can be used to correct for these discrepancies in the FD simulation.

The ν_e sample is made up of a number of background components, primarily NC and ν_μ-CC events, which must be corrected independently. By turning off the current in the NuMI beam focusing horns, the relative background contributions change in a well-modeled way, as shown in figure 1, allowing the individual components to be measured. After this correction the background consists of $(57\pm5)\%$ NC, $(32 \pm 7)\%$ ν_μ-CC and $(11 \pm 3)\%$ from CC interactions of the intrinsic ν_e beam background.

These background corrections are applied to the far detector simulation to give a total systematic uncertainty of 7.3% on the number of selected events, compared to a statistical uncertainty of 19%. An independent method of correcting the background takes the well-understood ν_μ-CC events and removes the muon from the reconstructed event to leave a well-understood sample of hadronic showers [4]. This produces consistent results.

4 Results

At the far detector, 35 ν_e-CC candidate events are seen. The expected background is 27 ± 5(stat.)±2(syst.) events. This is an excess of 1.5σ. The distribution of the selection variable (ANN) for these events is shown in figure 2, along with the reconstructed energy spectrum.

The best fit value for $\sin^2(2\theta_{13})$ is at the Chooz limit, and is dependent on the mass hierarchy (sign of $\Delta m^2_{\rm atm}$) and the CP-violating phase $\delta_{\rm CP}$. There is also a dependence on the values of $\sin^2(2\theta_{23})$ and $\Delta m^2_{\rm atm}$. All values quoted assume the MINOS best fit value of $\Delta m^2_{\rm atm} = 2.43 \times 10^{-3}\,{\rm eV}^2$ and $\sin^2(2\theta_{23}) = 1.0$ [5].

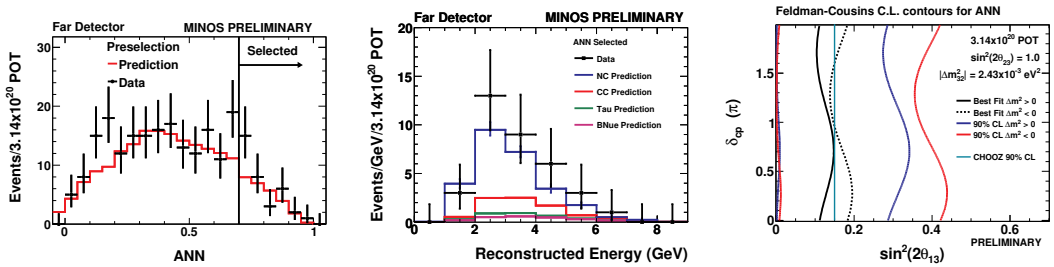

Fig. 2: Left: the distribution of the ν_e selection variable (ANN) for the far detector data (black), compared to the simulation after background correction (red); events to the right of the vertical black line are selected as ν_e-CC-like. Centre: the reconstructed energy spectrum of the selected ν_e-CC-like events in the far detector (black crosses), compared to the simulation after background correction (coloured, filled histograms) assuming $\theta_{13} = 0$. The various colours show the contributions from different backgrounds. Right: the MINOS 90% C.L. allowed regions for $\sin^2(2\theta_{13})$ for the normal (blue) and inverted (red) mass hierarchies. Also shown are the MINOS best fit values (black) and the Chooz 90% confidence limit [2] (grey).

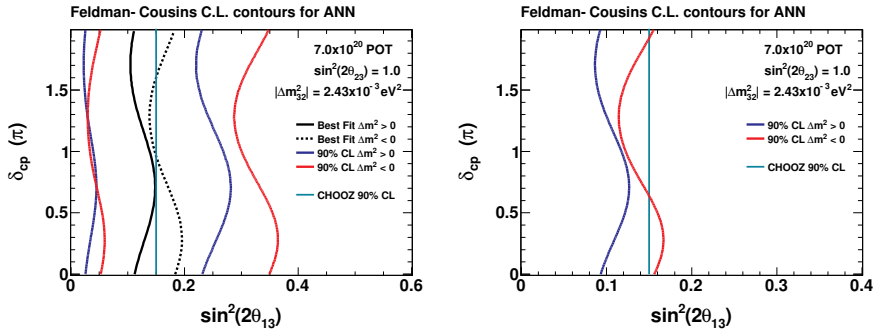

Fig. 3: The sensitivity of MINOS to $\sin^2(2\theta_{13})$ for an exposure of 7×10^{20} protons on target under two assumptions: left, that the observed excess persists in the new data; right, that there is no excess in the new data.

The 90% C.L. allowed regions for $\sin^2(2\theta_{13})$ are shown in figure 2. Assuming $\delta_{\rm CP} = 0$, MINOS allows $\sin^2(2\theta_{13}) < 0.29$ (90% C.L.) for the normal mass hierarchy, and $\sin^2(2\theta_{13}) < 0.42$ (90% C.L.) for the inverted hierarchy.

5 The future

The results presented here correspond to an exposure of 3.2×10^{20} protons on target (PoT). As of June 2009, MINOS has more than doubled this dataset, obtaining 7×10^{20} PoT. In early 2010, the analysis will be updated to include this new data. Figure 3 shows the sensitivity to $\sin^2(2\theta_{13})$ for this increased dataset, depending on whether the observed excess persists or goes away in the new data.

References

[1] D.G. Michael *et al.*, Nucl. Instrum. and Meth. **A596**, 190 (2008).

[2] M. Apollonio *et al.*, Eur. Phys. J. **C27**, 331 (2003).

[3] T. Yang, Ph.D. Thesis, Stanford University (2009).

[4] A. Holin, Ph.D. Thesis, UCL (2009).

[5] P. Adamson *et al.*, Phys. Rev. Lett. **101**, 131802 (2008).